William & Mary
CHARTERED 1693

W&M ScholarWorks

Dissertations, Theses, and Masters Projects

Theses, Dissertations, & Master Projects

2018

Radiation Shielding Bricks for Mars Using Martian Regolith Simulant and Hydrogen-Rich Polymers

Sara Sargent
College of William and Mary - Arts & Sciences, sesouthward@email.wm.edu

Follow this and additional works at: https://scholarworks.wm.edu/etd

 Part of the Chemistry Commons

Recommended Citation

Sargent, Sara, "Radiation Shielding Bricks for Mars Using Martian Regolith Simulant and Hydrogen-Rich Polymers" (2018). *Dissertations, Theses, and Masters Projects.* William & Mary. Paper 1550153774.
http://dx.doi.org/10.21220/s2-acwh-k853

This Thesis is brought to you for free and open access by the Theses, Dissertations, & Master Projects at W&M ScholarWorks. It has been accepted for inclusion in Dissertations, Theses, and Masters Projects by an authorized administrator of W&M ScholarWorks. For more information, please contact scholarworks@wm.edu.

Radiation Shielding Bricks for Mars using Martian Regolith Simulant and Hydrogen-rich Polymers

Sara Southward Sargent

Stanwood, Washington

B.S. of Chemistry, College of William & Mary, 2017

A Thesis presented to the Graduate Faculty
of The College of William & Mary in Candidacy for the Degree of
Master of Science

Department of Chemistry

College of William & Mary
August, 2018

© Copyright by Sara Sargent 2018

APPROVAL PAGE

This Thesis is submitted in partial fulfillment of the requirements for the degree of

Master of Science

Sara Southward Sargent

Sara Southward Sargent

Approved by the Committee May 2018

Committee Chair
Professor Emeritus Richard Kiefer, Chemistry
College of William & Mary

Professor of Chemistry Randolph Coleman, Chemistry
College of William & Mary

Chancellor Professor Christopher Abelt, Chemistry
College of William & Mary

ABSTRACT

Radiation shielding materials are an essential component of long-term space travel and habitation. The mission to Mars will require a radiation shielding material that can be produced on Mars through energy and cost-efficient means. In this study, Martian regolith simulant and hydrogen-rich polymers are used to create a radiation shielding material in the form of bricks. The bricks are capable of shielding against galactic cosmic radiation on Mars. There are three methods in which the bricks were formed: 1) a heated press, 2) a microwave oven in a CO_2 atmosphere, and 3) a vacuum oven with a low CO_2 pressure. Each brick varies by the type of polymer, percent of polymer, and the method in which it was made. Flexural tests were conducted on the bricks to determine the flexural strength, flexural strain, and modulus of elasticity. OLTARIS was used to estimate the effectiveness of these bricks to shield against GCR on the Martian surface.

TABLE OF CONTENTS

Acknowledgements ii

Dedications iii

Introduction 1

- Challenges of space travel and habitation 2
- Space radiation 3
- Effects of space radiation 7
- Protection against space radiation 9
- Experimental considerations 12
- Our proposed solution 12

Experimental 13

- Materials 13
- Methods 17
- Flexural tests 25
- OLTARIS 26

Results/Discussion 29

- Method analysis 29
- Flexural tests 31
- OLTARIS 41

Conclusion 52

Appendix 54

References 63

ACKNOWLEDGEMENTS

I wish to thank Dr. Richard L. Kiefer for his support, guidance, and mentorship during my time as both a Master of Science degree student and Bachelor of Science degree student. Additionally, I wish to honor the memory of Dr. Robert Orwoll who was my undergraduate research advisor and foundational in my understanding of polymer chemistry. I am grateful for the experiences I have had in the lab and through our collaborations with colleagues from NASA and International Scientific Technologies, Inc.. In particular, I would like to thank Martha Clowdsley and Chris Sandridge for their help with using OLTARIS and Eugene Aquino for his discussions about the bricks. I would like to give a special thanks to Julia Romberger and Liz Weech for their help with making bricks, along with Logan Feierbach and Will Park for setting the groundwork for this project.

This Master's thesis is dedicated to my loving mom who has inspired my love for school and chemistry and additionally, to my Godfather for his unfaltering support and encouragement.

INTRODUCTION

In recent years, scientists have worked towards a common goal of sending humans to Mars. A similar goal was achieved on July 20, 1969, when Neil Armstrong and his Apollo 11 crew successfully landed and walked on the Moon.[1] This mission was impressive in itself and ultimately set the groundwork for future endeavors such as the mission to Mars. However, there are enough differences between the Moon and Mars that different technology, instrumentation, and strategies must be used in order to make the trip a safe and successful one.

On a mission to Mars, astronauts will experience increased amounts of galactic cosmic radiation (GCR) in transit and after landing. Once on Mars, astronauts will need protection from this radiation as well as a structural material to build and repair their habitats. This paper proposes using readily available Martian regolith combined with a polymer that will act as a binding agent and provide radiation protection. Due to the weight and space limitations of current spacecrafts, as well as the lack of harnessed energy sources in space, we further propose production technologies that are energy-efficient, light-weight, space-saving, and portable. Ultimately, these materials can be shaped into versatile bricks which will provide suitable protection against GCR, making possible long-term space habitation.

Challenges of space travel and habitation

Identifying the challenges of space travel and habitation are important for developing procedures and technologies that will be responsive to the space environment. To begin, it is important to know that the distance from the Earth to Mars is much greater than that from the Earth to the Moon. The distance between the Earth and the Moon ranges between 226 to 252 thousand miles,[2] not even a hundredth of the distance between the Earth and Mars. At their closest distance, the Earth and Mars are around 33.9 million miles apart and at their furthest distance, with the sun located between them, they are 250 million miles apart. This means that the mission and space launches will have to be carefully timed so that the planets are at their closest distance to each other. The optimal difference occurs once every 26 months.[3] With current technology, the most energy-efficient trip to Mars will take about nine months.[4] However, making the trip in six months, though less energy-efficient, will decrease the radiation exposure time.

Due to the orbits of the planets, the astronauts will have to remain on Mars for nearly two years before the planets will be close enough for the astronauts to embark on the return journey home. This means that the astronauts will have to be capable of repairing any type of damage or mechanical failure that occurs while there. They will be in charge of gathering and analyzing data from the Martian terrain. Furthermore, if any telecommunication from Earth is needed, the astronauts will experience at least

a 40 minute delay for sending and receiving signals.[5] Therefore, the astronauts will need to be extremely educated and self-sufficient in order to complete all the tasks that such a mission will present.

The leading deterrent and, ultimately, the driving force for this research, is the radiation in space. Astronauts, space electronics, and instruments are all susceptible to the detrimental effects of space radiation. Long-term missions, such as the one to Mars, increase the radiation-exposure time, further intensifying its effects. While it is important that the spacecraft and the cargo inside are properly protected against from the radiation on the journey to Mars, our focus will be to protect against the radiation while there. In order to develop radiation shielding materials suitable for this purpose, it is important to first understand what space radiation is and why it is dangerous.

Space Radiation

There are two forms of radiation in space that are major concerns for long-distance space travel and habitation: solar energetic particles (SEP) from solar winds/solar particle events (SPE) and galactic cosmic radiation (GCR). Radiation from the near ultra-violet (UV), visible, and infrared parts of the electromagnetic (EM) spectrum are forms of non-ionizing radiation[6]. Non-ionizing forms of radiation lack the necessary energy required to remove electrons from other atoms and molecules, making them less dangerous and easier to shield against.[7] Radiation in the form of gamma rays, X-rays, and

from the higher energy UV region of the EM spectrum are all forms of ionizing radiation. They pose a larger threat because they contain the necessary energy to remove electrons from the orbits of atoms and molecules. Furthermore, ionizing radiation can cause atoms or molecules to become highly reactive charged particles, which can instigate a chain reaction of molecular breakdown. For space travel and habitation this means that astronauts, space-crafts, and instrumentation are all at risk of serious damage upon exposure.

The sun is a major source of space radiation and produces what is known as a solar wind: a constant emission of protons, electrons, alpha particles, and heavy particles. The solar wind travels through space and creates a bubble around the planets known as the heliosphere.[8] Due to solar winds, space around Earth is filled with magnetic fields and radiation that all trace back to the sun. The sun experiences different levels of activity, marked by the frequent occurrence of solar flares and coronal mass ejections. When these occur, particles become accelerated to high speeds with increased energetic potential. The energies of these particles have a range depending on the magnitude of the event and the type of particle emitted. Typically, the energy of solar-produced ions is below 1 GeV with rare occurrences surpassing 10 GeV.[9] When SPEs occur, the amount of particles released increases, generating an intense wave of energetic particles over short periods of time. Solar particle events occur more frequently during a solar maximum, which lasts a span of

seven years in an eleven-year min/max cycle.[10] A solar maximum refers to the increased activity of the sun and is further identified as the greatest number of sunspots which occurs during the solar cycle.[11] During these active solar periods, GCR is at minimum. This is due to the fact that the interplanetary magnetic field is disturbed by the sun's activity. The irregularities of the magnetic field cause the energy of the GCR to be reduced and the rays to be scattered. Overall, this lowers the flux and intensity of the particles.[12] GCR is much more difficult to shield against than radiation from the sun and so, timing space missions during solar maxima is important.

Galactic cosmic radiation is the most detrimental to life and instrumentation in space. GCR consists of high energy particles which have been stripped of all their electrons from traveling through galaxies at high velocities approaching the speed of light.[13] The energy of these particles can be many GeV greater than solar particles.[14] Galactic cosmic particles ionize as they pass through matter, knocking off more than just an atom's valence electrons. GCR is primarily composed of hydrogen and helium particles, however, GCR particles do exist as heavier elements. *Figure 1* shows the elemental composition of GCR relative to the elements in the solar system. Interestingly, light-weight elements such as lithium, beryllium, and boron are not common in our solar system, yet are very common in GCR. Scientists speculate that these elements were the product of heavier GCR particles, which collided with gas in interstellar space.[15]

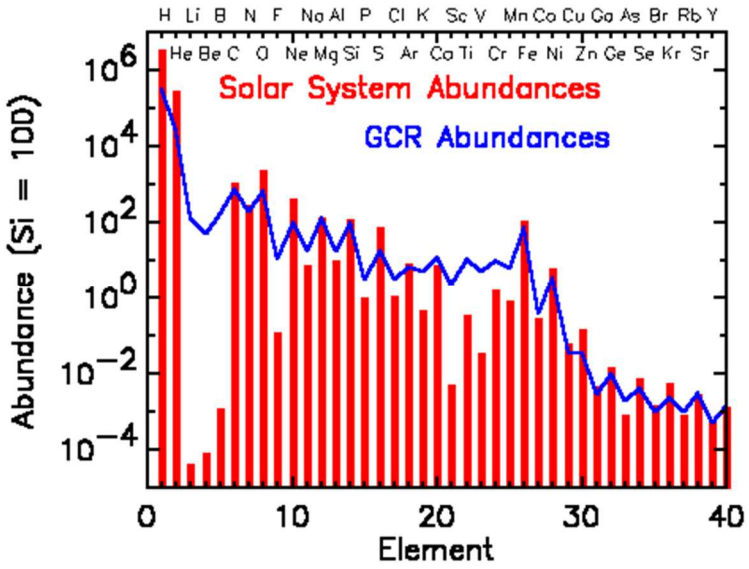

Figure 1. Elemental composition of galactic cosmic radiation compared to the elements that are abundant in the solar system. Silicon is used as a reference because it is easy to measure. Figure from NASA.[15]

When GCR particles collide with the nucleus of heavy atoms, they can cause the target nucleus to break apart into smaller nuclei. The products become a secondary source of radiation and can penetrate through materials, increasing the radiation dose that the material receives. Heavier elements are more susceptible to becoming a source of secondary radiation, because they are larger and contain a nucleus that can be broken apart. Neutrons that are knocked out of an atom's nucleus, by a GCR, are dangerous, because of their absorbed energetic potential and lack of charge which allows them to pass through matter with ease. Further analysis of neutron radiation damage is outside the scope of this study and will not be discussed. Overall, GCR remains the leading deterrent for space exploration and will be the subject of

this research which proposes developing materials capable of shielding against GCR on the Martian surface.

Effects of space radiation

While space radiation causes havoc to a number of systems in space, including electronics and spacecraft, the most important concern is how radiation affects humans. On Earth, a human receives an average yearly effective dose of 0.0062 Sieverts (Sv). Part of this radiation comes from small amounts of cosmic rays and radon in the air; the other part comes from medical and industrial sources.[16] Sieverts are a unit of radiation which takes into account the amount of radiation the person receives, as well as the type of radiation and the amount of damage that that radiation can do. For two equal absorbed doses of radiation, if one dose causes more damage, it will have a higher Sievert value.[17]

In space, radiation in the form of particles can damage DNA and cause acute radiation sickness or cancer.[18] Acute effects from radiation occur immediately after exposure to a large amount of radiation. The symptoms include vomiting, headaches, dizziness, and fatigue. Chronic symptoms appear at varying lengths of time after exposure occurs, and result in various forms of cancers or other diseases. These symptoms are caused by exposure over extended periods of time. [19]

The Mars rover Curiosity has allowed scientists to calculate the

expected radiation dose that an astronaut would receive on a round-trip mission to Mars. Curiosity is equipped with a three-pound Radiation Assessment Detector (RAD), which provides information about the radiation particle types and related frequencies of the radiation on the Martian surface.[20] On its 253-day journey to Mars, the Curiosity rover was subjected to an average of 1.84 mSv of GCR particles per day. With current technology, an astronaut on a 253-day journey would be subjected to an average of 331 ± 54 mSv on the journey to Mars; including the return-trip that number would double to 662 ± 108 mSv.[21] Once on Mars, that number would further increase. *Figure 2* shows the average radiation dose equivalent for: an American, a radiation worker, a 180-day trip to Mars, and a 500-day stay on Mars. After 500 days on Mars, an astronaut will have been exposed to around 300 mSv of radiation. It is worth noting that radiation doses in space can vary depending on unpredictable solar flares.

NASA will only let their astronauts experience a radiation dose that causes a 3% increase in the astronaut's chance of developing fatal cancer. Typically, a radiation dose of 1 Sv experienced over time causes a 5% increase in fatal cancer. [22] Current technology does not give adequate protection against the radiation in space and astronauts would surpass the exposure limit. This further confirms the need for radiation shielding materials.

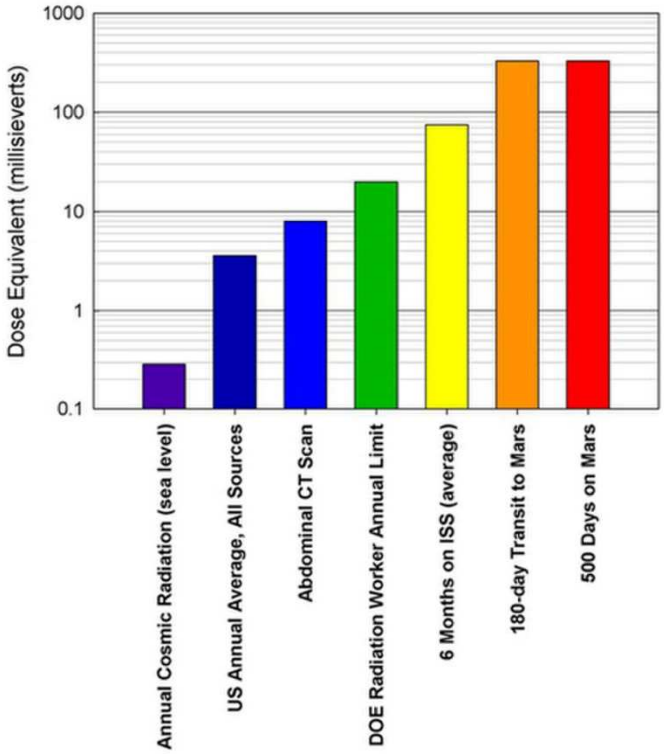

Figure 2. Comparison of radiation dose equivalents experienced on Earth and on Mars. Figure from Sheyna E. Gifford, but credited to NASA, JPL. [23]

Protection against space radiation

Earth is protected from most space radiation due to the magnetosphere. Our planet has a molten iron core which generates a magnetic field and deflects the majority of incoming particles.[24] *Figure 3* depicts how the magnetosphere shields against incoming particles from the Sun. Some particles can be captured by the magnetic field and become trapped in what are known as the Van Allen radiation belts. Mars does not have a magnetosphere to protect against space radiation. Furthermore, Earth's atmosphere adds further protection against space radiation, while Mars' very thin atmosphere does not

provide such protection. For these reasons, radiation shielding is essential for a mission to Mars to be possible.

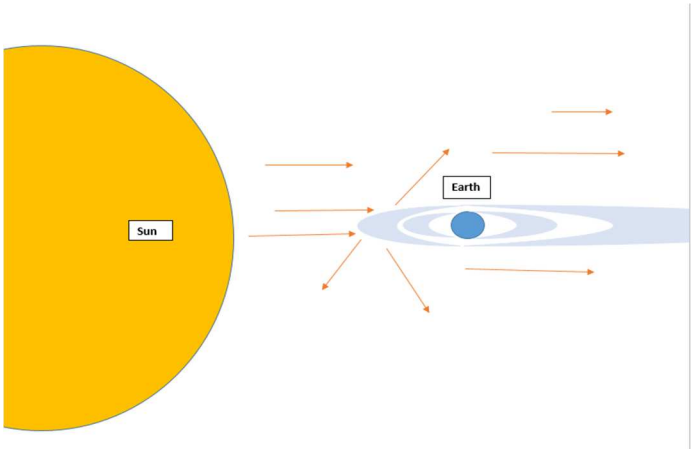

Figure 3. Picture of Earth's magnetosphere protecting Earth from radiation from the Sun.

There are many factors that must be considered when developing a radiation shielding material which can be used for habitat construction on Mars. As will be discussed, the terrain on Mars is barren, lifeless, and essentially rocky soil. The resources brought to Mars on the spacecraft will have to be used wisely and frugally, for they cannot be replenished. Minimizing the amount of material necessary for the radiation shield will not only save room on the spacecraft for essential items such as food and water, but it will also cut down on the overall cost of the mission. As the weight of the spacecraft increases, the cost of the operation increases and for this reason, we want to utilize light-weight materials.

Typical radiation shields utilize heavy elements to block against

radiation. However, this will not effectively protect against GCR and SPE, due to the build-up of secondary radiation that could occur on the inside of the shield. In addition, neutrons that are emitted after the collision of a galactic cosmic ray particle with a nucleus, are capable of passing through dense materials.[25] The logic behind the shield proposed in this paper stems from Coulomb's Law which states that unlike charges attract. Therefore, a shield that consists of high electron density materials will most effectively protect against GCR and SPE, which consist of positively charged nuclei. The electrons in the shield will interact coulombically with the incoming nuclei, absorbing the high kinetic energy upon impact. The nuclei of elements with a large atomic number also can be broken apart by a collision with the incoming particle. Therefore, we are looking to use light-weight elements in the shield.

Hydrogen is the best-known element to protect against ionizing radiation, such as GCR. It contains no neutrons, which in other elements adds weight but no more charge to interact electrostatically with the incoming nuclei.[26] Additionally, hydrogen has the highest electron density per unit mass, and its nucleus cannot be broken into smaller particles. Therefore, secondary radiation will not be as high a concern with a hydrogen-rich material. The incident charged particles in GCR will lose energy primarily through the Coulombic interactions with the electrons in the shield.

Experimental Considerations

There are numerous differences between the Earth and Mars and knowing these differences will be particularly useful when designing methodologies to create the radiation shielding materials. In regard to this research, the atmospheric pressure at surface level, atmospheric mass, and atmospheric composition of Mars will be applied to the experimental set-up in ways which emulate the Martian environment. First-off, the mass of Mars's atmosphere, which is about $2.5x10^{16}$ kg, is 0.49% of Earth's atmospheric mass of $5.1x10^{18}$ kg. The atmospheric surface pressure on Mars at the mean radius is 6.36 mb. On Earth, the atmospheric surface pressure is 1014 mb. Mars has an atmospheric surface level pressure that is 0.6% of Earth's. Mars' atmosphere is composed of the following gases: 95.32% CO_2, 2.7% N_2, 1.6% Ar, and 0.13% O_2. In comparison, Earth's atmosphere consists of 78.08% N_2, 20.95% O_2, 9340 ppm Ar, and 400 ppm CO_2.[27,28] These are just a few of the many differences between Mars and the Earth, however, these will be the most useful for our experimental design.

Our proposed solution

On a spacecraft, space is limited and minimizing weight is important. For these reasons, we want to utilize the materials available on Mars and minimize the amount of materials that must be taken up into space. A suitable radiation shielding material can be produced using Martian regolith and

hydrogen-rich polymers. Hydrogen-rich polymers can effectively protect against space radiation, and in particular, galactic cosmic radiation. The combination of these materials can be molded into bricks and built into structural units, which protect humans, electronics, and other materials from the radiation in space.

EXPERIMENTAL

Materials

Polymers

The polymers used in this study include: low-density polyethylene (PE), polyethylene oxide (PEO), polycaprolactone (PCL), and an epoxy powder. PE, PCL, and PEO are all hydrogen-rich polymers with properties that make them suitable for a radiation shielding material. In addition, the epoxy powder was used because of its good mechanical properties and ease of mixing with the regolith. All of these polymers were used in this study in combination with a simulated Martian regolith in order to construct radiation-shielding bricks for Mars. The polymers served two purposes: 1) to provide the hydrogen content capable of shielding against space radiation, and 2) to act as an adhesive to hold the bricks together. The epoxy powder was purchased from Hapco, Inc., and is called Sympoxy 1960G (SYM). The structure for SYM is proprietary. It is a one-component, epoxy powder that has a curing temperature of 150^{o}C. Polycaprolactone was purchased from Polysciences, Inc.;

polyethylene from Alfa Aesar; and polycaprolactone from Sigma Aldrich. The melting temperatures for PE, PEO, and PCL are 110 ºC, 65 ºC, and 60 ºC, respectively. In the same order, the percent hydrogen contribution from each polymer is as follows: 14.37% (PE), 9.15% (PEO), and 8.83% (PCL). All of the polymers are readily available and inexpensive to purchase. *Figures 4, 5, and 6* show the structures of each polymer.

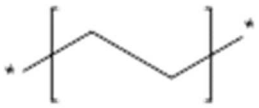

Figure 4. Polyethylene

Figure 5. Polyethylene oxide

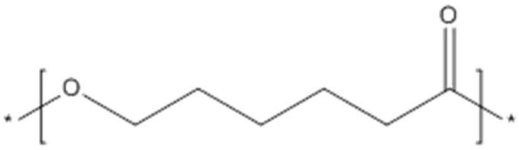

Figure 6. Polycaprolactone

Martian regolith simulant

In this study, two types of Martian regolith simulant were used. Earlier trials were conducted using a Martian regolith simulant known as JSC-Mars-1A regolith. It contains weathered ash from the Pu'u Nene volcano on the Island of Hawaii. The JSC-Mars-1A regolith simulant was compared to Martian regolith found at the Viking and Pathfinder sites and to VIS/NIR reflectance spectra of the bright regions on Mars. While the simulant is similar to Martian soil in composition, it contains volatiles and enhanced magnetic

properties which are not present in the Martian soil.[29] This product was discontinued and the brick trials were resumed using a different simulant known as the Mojave Mars Regolith Simulant (MMRS). Since the JSC-Mars-1A was known to be volatile, we conducted a thermal analysis on the two types of regolith simulants using a thermal gravimetric analysis instrument (TGA). A sample from the remaining batch of JSC-Mars-1A regolith, and from the MMRS, were placed in a vacuum oven at 110 ºC for five days. They were transferred to a vacuum-sealed desiccator so as not to absorb moisture before the TGA testing occurred. Samples from both types of regolith that were not dried in the vacuum oven were also tested. All of the regolith samples were heated to 1000 ºC under nitrogen gas. The results of this experiment are depicted in *Figure 7.*

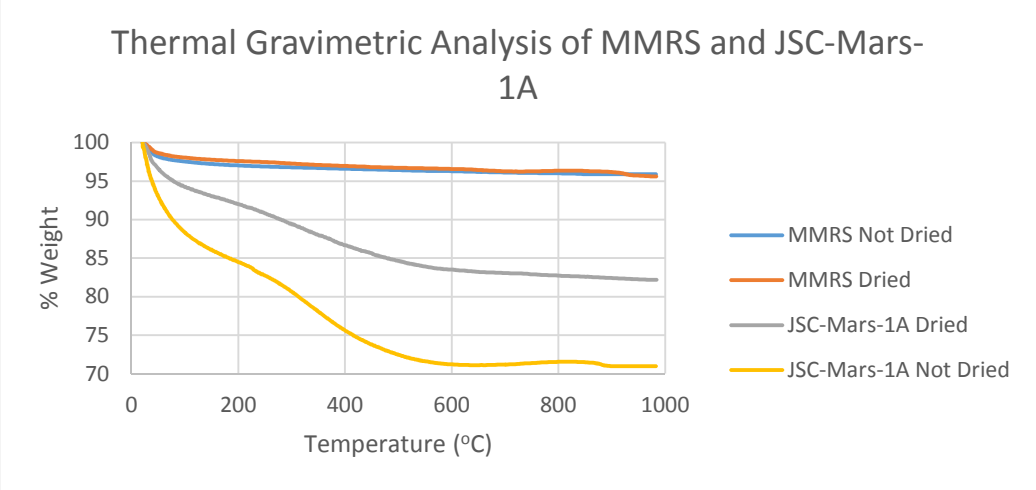

Figure 7. Thermal gravimetric analysis of MMRS and JSC-Mars-1A dried and not dried.

As expected, the TGA data from the JSC-Mars-1A samples show that the oven dried sample lost 18% of its initial mass by the time it reached 1000 ^{o}C compared to nearly a 30% loss when the sample was not dried. This confirms that the JSC-Mars-1A simulant contains volatile components. The decrease in mass is due to a loss of water and most likely SO_2.[29] In comparison, the Mojave Mars Regolith Simulant shows almost no difference between the dried and non-dried samples. At 1000 ^{o}C, the samples lose less than 5% of their initial weight. This data indicates that the Mojave Mars Regolith Simulant absorbs almost no moisture when exposed to the air and the likelihood of any gases being exuded are low. Therefore, the TGA test results affirm our decision to use the Mojave Mars Regolith Simulant for all samples made during this project.

Table 1. Comparison of the Martian Regolith Simulants to the chemical composition of Mars.[30]

Oxides	**Mars[1] (ave wt%)**	**JSC-1A (wt%)**	**MMRS (wt%)**
SiO_2	43.9	43.5	47.9
Fe_2O_3 and FeO	18.1	15.6	10.6
Al_2O_3	8.1	23.3	16.7
MgO	7.1	3.4	5.9
CaO	6.0	6.2	10.4
Na_2O	1.4	2.4	3.3
Cr_2O_3	0.2	----	0.05

As can be deduced from *Table 1,* both Martian regolith simulants contain similar oxide concentrations to the soil found on Mars at the Viking

and Pathfinder sites. In addition to the oxide components, the Curiosity rover found water and trace amounts of chlorobenzene and dichloroalkanes after drilling into the mudstone at its landing site, the Gale crater.[31] However, the majority of the planet is barren and contains no life or organic material. Due to the planet's lack of a magnetosphere, Mars has little to no protection against space radiation. Therefore, solar winds strip the planet's atmosphere of gases and make the planet unable to sustain life or organic material.

Methods

Brick preparation

Each brick mixture was prepared using a standardized procedure. An individual brick had a mass of 20 grams and was composed of either 10% polymer or 20% polymer, with the remaining contents consisting of the Mojave Mars Regolith Simulant. Six brick specimens were made for each of the four polymers at both 10% and 20%. This procedure was repeated using three different production methods (described below) to generate a total of 144 bricks. This number of specimens was necessary for the flexural tests that were conducted. The contents were carefully measured on a balance and then blended in a coffee grinder for 20 seconds to ensure thorough mixing. Afterwards, the mixture was poured into an appropriate brick mold, dependent on the method used. The mold was sprayed with an even layer of a releasing agent called Grease It Five, purchased from Hapco, Inc. This prevented the

polymer from adhering to the mold.

Both the vacuum oven and heated press required the use of a steel mold, pictured in *Figure 8*. A steel mold was preferable because it could withstand the temperatures and pressures used in this study. The dimensions of this mold were 0.75 inches wide by 3.5 inches long, with a maximum depth of 0.73 inches. This depth varied based on the components of the brick mixture. The mold was held together by steel screws and was easy to assemble.

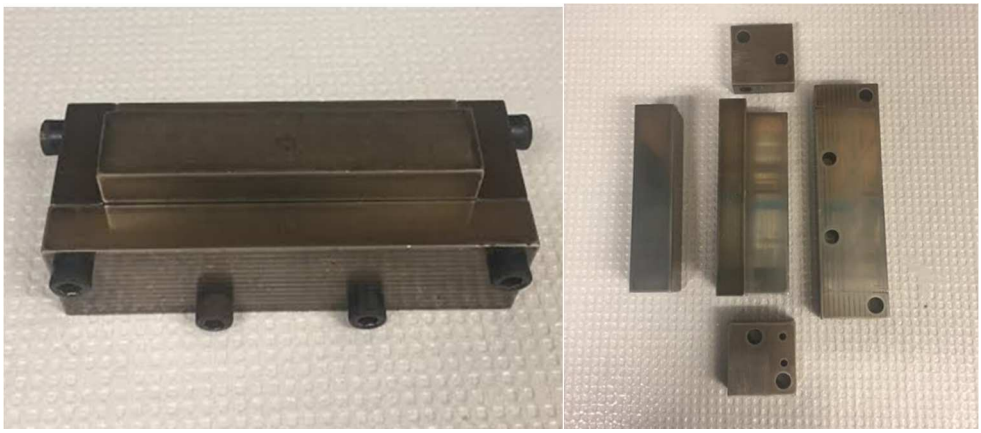

Figure 8. Steel mold used for the bricks created in the vacuum oven and heated press (fully assembled, left; not assembled, right).

The microwave method required the use of another type of mold, since steel cannot be microwaved. Initial trials were conducted using a mold constructed from ULTEM, pictured in *Figure 9*. ULTEM is a polyetherimide material which is known to have good mechanical properties such as heat resistance, solvent resistance, and flame resistance.[32] Its glass transition temperature is 217 ^{o}C, well above the melting temperatures of the polymers

used in this study. This mold was held together by ULTEM rods, an epoxy glue, and was wrapped in Kapton tape for further support. Despite its acclaimed properties, this mold experienced a few issues during the microwave trials. For one, areas of bubbling occurred, which was attributed to hot spots generated by the microwave and uneven heating. Second, the ULTEM molds started to exhibit stress cracks, which may have resulted during the cooling process. Last, it was difficult to keep the mold from falling apart. While a high heat resistant glue was necessary to hold certain parts together, a releasing agent was also necessary so the brick did not adhere to the mold. Unfortunately, the releasing agent was specifically developed to release epoxies and our efforts were counter effective.

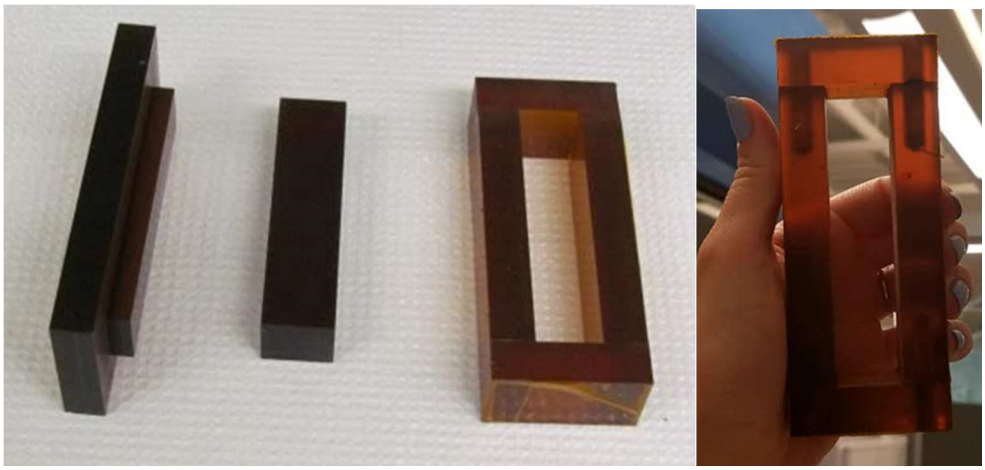

Figure 9. ULTEM brick mold used for initial microwave trials.

Due to the many issues with the ULTEM mold, a mold was crafted out of Teflon, pictured in *Figure 10*. Teflon is composed of polymerized

tetrafluoroethylene and has a high melting temperature of 335 ^{o}C. This mold was specifically designed to have fewer parts to fit together. Therefore, no posts or glue were required. Overall, this mold worked well for this method and showed no signs of mechanical failure through bubbling or cracking. The dimensions of this mold were 0.75 inches wide by 3.5 inches long and 0.73 inches deep.

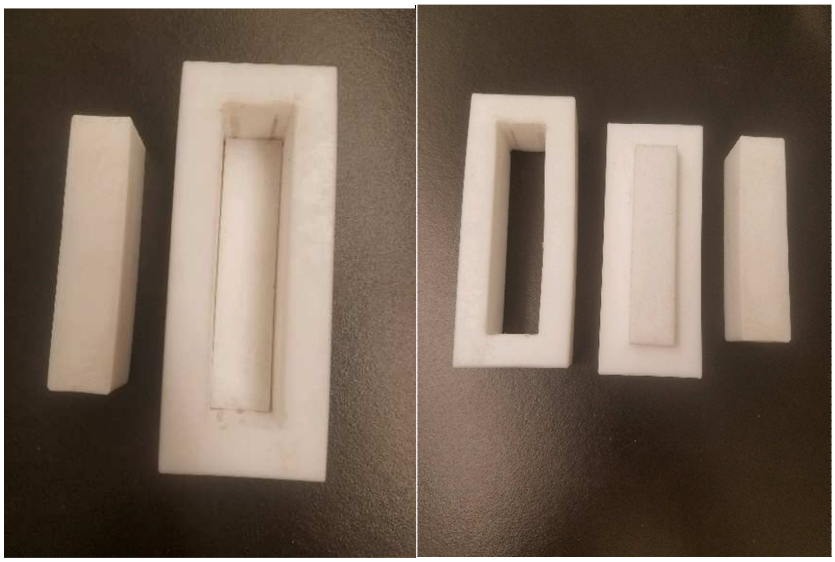

Figure 10. Teflon brick mold used for the microwave trials (partly assembled, left; not assembled, right).

Heated hydraulic press method

The brick specimens created for the hydraulic press were prepared in a steel mold and placed in the press (see Figure 11). Based on the polymer's melting or curing temperature, the specimen was heated to the appropriate temperature and pressed at 300 psi for 90 minutes. Afterwards, the brick

cooled under pressure until the temperature dropped below the melting or curing temperature. It was allowed to cool further at room temperature for a few hours. It is necessary to mention that the pressure was manually applied and though care was taken while making the bricks, the pressure sometimes spiked to higher levels than intended. The temperatures used for the heated press and vacuum oven are contained in *Table 2*.

Table 2. Temperatures used for making the bricks in the vacuum oven and heated press.

Polymer	PCL	PEO	PE	SYM
Temperature (Celsius)	100	100	150	160

Figure 11. Heated hydraulic press experimental setup.

Microwave in a CO_2-filled glove box

Brick specimens created for the microwave method were prepared as previously described. After preparation, the mold was placed into the air lock which is the small box on the right side of the main chamber seen in *Figure 12*. The air lock was then filled with CO_2 for a couple of minutes before the specimen was transferred into the main CO_2 chamber (prefilled with CO_2). A large evaporating dish filled with about an inch of sand was microwaved at power 10 for 10 minutes. The purpose of the sand was to supply an additional material to absorb heat while the brick was being microwaved to reduce the risk of hot spots. Initially, this was done on a trial basis and proved successful, so we continued to do this. Microwaving the sand beforehand ensured that while the brick was heating, the sand would not absorb the majority of the heat and the brick could still heat. Early trials show that heating the bricks at a low power for a longer period of time, rather than a high power for a shorter period of time, allowed for the brick and polymer to cure without ruining the mold. The microwave is capable of running at powers 1-10, but we found that all of the polymers were able to melt/cure after 30-60 minutes at power 6. Once the microwave trial was complete, the regolith/polymer brick was removed from the microwave and cooled with a fifteen-pound lead brick placed on top of it, while still remaining in the CO_2 atmosphere.

The bricks from this method were constructed in a CO_2 atmosphere in

order to simulate the atmosphere on Mars. Ideally, a vacuum would also be applied to account for the low atmospheric pressure. However, vacuum conditions in a glovebox are not feasible because the gloves would implode. Furthermore, it was suggested by microwave manufacturers that the microwave may not function under vacuum conditions and a special one would need to be designed.

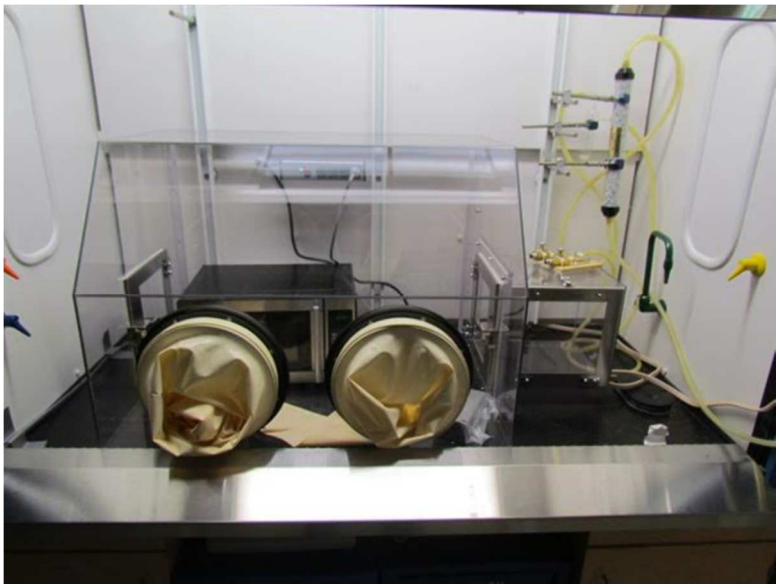

Figure 12. Microwave in a CO_2 atmosphere experimental setup.

Vacuum oven under low CO_2 pressure

Brick specimens created for the vacuum oven were prepared as previously described and then loaded into the oven. A fifteen-pound lead brick was placed on top of the mold during the heating process, which amounts to 5.71 psi. The oven door was closed and the air was evacuated using the house

vacuum system. Once the pressure gauge was at a minimum, the vacuum was shut off and the oven was pumped full of CO_2 until the pressure gauge displayed that the oven was re-pressurized to 1 atmosphere with CO_2. This process was repeated two additional times to ensure that the oven was depleted of air. Lastly, the CO_2 pump was closed and the vacuum was opened. This ensured that the brick could be produced in an environment of low CO_2 pressure. As in the other methods, the temperature was set according to the melting or curing temperature of the polymer. The brick was heated for 1.5 hours and was removed to cool at room temperature until cool to the touch.

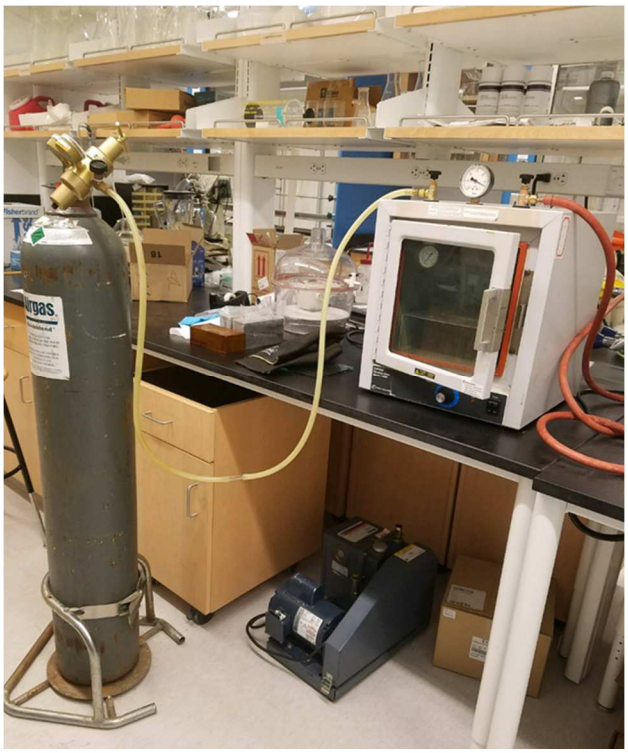

Figure 13. Vacuum oven under low CO_2 pressure setup.

Flexural Tests

Flexural tests were performed on the bricks using an Instron 5848 Micro Tester to determine the mechanical properties. Six brick specimens were prepared for each type of polymer (PE, PCL, PEO, and SYM) at a 10 % polymer weight and a 20 % polymer weight. A total of 48 bricks (6 trial bricks, 4 polymers, 2 polymer weight percentages) were created for each method. Though the confinements of the brick mold control for large variations in size, the width and thickness of each brick were individually measured with a micrometer to enhance the accuracy of the tests. The measurements for the bricks can be found in *Tables S1, S2,* and *S3* (refer to appendix). These values were entered into the computer before the flexural tests began.

The Instron 5848 Micro Tester was assembled with a ±1 kN static load cell, which is a transducer that converts a force value into an electrical signal that the computer can read.[33] On top of the load cell sat a rod with an attached bar and two support beams. For each trial, the support span distance remained constant at 22.07 mm. A rod attached to the top of the instrument had an attachment called the loading nose, which was centered between the support beams. The purpose of this piece was to apply the force to the test specimen that was sitting on the support span. *Figure 14* gives a visual representation of the setup for the flexural tests.

Figure 14. Flexural test setup on the Instron 5848 Micro Tester.

Before testing, the instrument was calibrated and after the brick was carefully centered on the support beams, the gauge length was reset and the balance zeroed. Once the test began, the loading nose moved down towards the specimen at a crosshead motion rate of 0.5 mm/min and applied a force until the brick ruptured or a maximum strain was reached. Load-deflection data was recorded as the experiment occurred and was later uploaded into Excel so that it could be plotted.[34]

OLTARIS

OLTARIS (On- Line Tool for the Assessment of Radiation in Space) is

a NASA-developed program used to study the effects of space radiation on shielding materials. For our purposes, we used this tool to form a general idea of the protection the bricks would offer astronauts against GCR on Mars. In order to do this, we uploaded the molecular percentages of our materials into the program and used NASA's molecular composition for Martian soil rather than that of MMRS. As an example, a brick composed of 10% PCL and 90% Martian regolith had the following molecular percentage breakdown: 10% $C_6H_{10}O_2$ (PCL), 6.66% H_2O, 28.89% $Al_2CaK_2MgNa_2O_7$, 8.37% Fe_2O_3, and 46.08% O_2Si. Only the brick compositions involving PEO, PCL, and PE were used for the OLTARIS simulations. Since the composition of SYM is proprietary, we could not upload it as a material and generate results.

This program has limited geometries available for modeling materials on the Martian surface. Therefore, our only option was to model our material around an astronaut as a sphere. Specifically, a "Thickness Metafile format" had to be created to define the sphere with a set number of rays, which are used to trace the radiation at certain locations on the sphere. This file is called a "thickness distribution". It defined the geometry of the sphere in regards to the number of rays, the material used, the density of the material, and the thickness. The spheres in our calculations included 968 rays. After uploading our materials and thickness distributions, we set up "projects", which carry out the calculations and radiation analysis.

To run a project we chose from a variety of environments, geometries,

and response functions. The available environments included SPE (solar particle events) or GCR in all of the following: free space, on the lunar surface, or on the Martian surface. For obvious reasons, we chose to model our materials in a GCR environment on the Martian surface. The next step involved choosing the correct thickness distribution, previously described. From there we chose the mission parameters to be: an elevation of 0 km, which is equivalent to sea level on Earth, and a mission duration of 1.0 day.

Seven response functions were available to choose from. These are the radiation calculations the program computes. We chose to compute the dose, dose equivalent, and effective dose equivalent. Dose was calculated in tissue (rather than silicon) whose units are reported in milliGray (mGy), since the focus of this research is on protecting humans. The value generated for this calculation showed the amount of energy deposited in the target material (astronaut) after traversing the shielding material. Dose equivalent takes into account the type of charged particles that produce the absorbed dose and the effect they have on human tissue. Since different types of radiation particles will have different effects on tissue, this calculation required the use of what are known as quality factors. Quality factors weight the impact of the charged particle based on the type of radiation. In this simulation, NASA Q quality factors were used for the dose equivalent calculations, which computed two dose equivalent values for two types of cancer caused by radiation, leukemia and solid cancer. The last calculation computed was the effective dose

equivalent. In this calculation, the target material (tissue) is weighted, rather than the source (type of charged particle). Each organ in the body responds differently to radiation and some are more susceptible to damage than others, so each organ has a different "weight". The weighted sum of the average radiation experienced by the organs produces the effective dose equivalent. The units for this measurement are in mSv.[35]

RESULTS/DISCUSSION

Method analysis

Each brick was made using one of the three methods previously described. *Figure 15* depicts what the final products look like. Overall, the heated hydraulic press generated the most durable and clean specimens, while the vacuum oven and microwave produced bricks that were sometimes rough around the edges, more likely to crumble, and uneven. Despite this, each method was used to produce samples and only the bricks which had even thickness and which maintained their shape were tested.

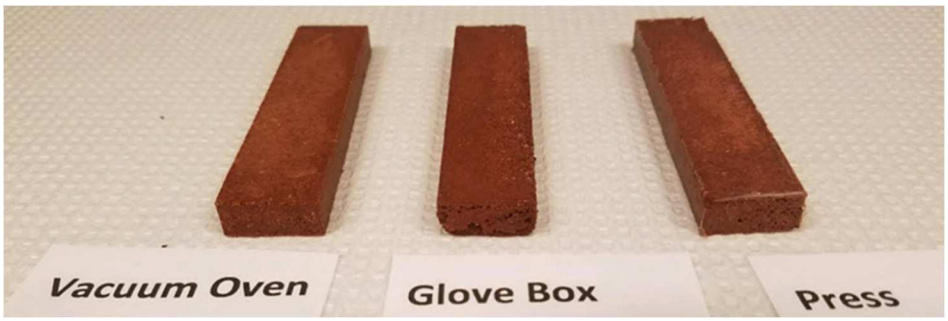

Figure 15. Brick specimens created using the vacuum oven, microwave in a glovebox, and the heated press.

Both the vacuum oven and microwave methods incorporated features to simulate brick production in a Martian environment; the vacuum oven bricks were made under low CO_2 atmospheric pressure and the microwave bricks in a CO_2 atmosphere. The amount of pressure applied during the heating process is the primary difference between all of the methods. The heated hydraulic press method involves a higher amount of pressure than the other methods, and for this reason, produces more desirable bricks. While this method produces the best substrates, it is not a viable option to use in space due to the weight of the instrument. Conversely, both the vacuum oven and microwave are energy-efficient, lightweight options. Despite being a less attractive option, the heated press gives valuable insight into how pressure affects the mechanical properties and quality of the bricks. In the future the results from this study could be used to develop a different method, which incorporates high amounts of pressure.

While preliminary brick trials had included making 5%, 7.5% and 15% polymer bricks in addition to 10% and 20%, the number of specimens necessary for the flexural tests caused us to choose two polymer percentages to study. The most attractive of all the options are 10% and 20% because the majority of the bricks held together with these polymer percentages. Furthermore, these percentages provide a large enough disparity that we can still identify differences between the mechanical properties of the bricks. 5% polymer was not enough to bind the regolith together, but there were a few

successful trials for 7.5% PE bricks. Additionally, a wetting agent was used for mixing in earlier trials, but was deemed an unnecessary addition and not continued. Lastly, several polymer blend bricks were made successfully, the best results coming from a 50/50 mixture of 10% PE and 10% SYM. However, for simplicity we chose not to pursue testing of these blends.

Flexural tests

As mentioned previously, each brick was tested using the Instron 5848 Micro Tester to determine the flexural properties of the material. *Table 3* contains the average maximum load values in Newtons (N) that the bricks withstand before breaking or yielding. These values were calculated using the load-deflection data obtained during the flexural tests. *Table S4* contains all of the maximum load data points for the samples tested.

Table 3. Average maximum load values (N).

10% Polymer weight, average load (N)				**20% Polymer weight, average load (N)**			
	VO	**HP**	**GB**		**VO**	**HP**	**GB**
PCL	75.078	189.001	70.858	**PCL**	260.942	376.445	268.799
PE	65.063	122.606	73.641	**PE**	257.072	294.630	261.493
PEO	21.357	43.581	16.257	**PEO**	114.520	167.088	105.730
SYM	144.898	165.839	26.460	**SYM**	293.689	390.032	97.678

The average maximum load values for the brick specimens created in the heated hydraulic press are significantly larger compared to those of the bricks made by the other methods. We deduce that this method generates the

strongest bricks. Furthermore, the percent of polymer also affects the strength of the brick, with 20% polymer bricks withstanding a larger load than the 10% polymer bricks. A less noticeable, but important detail, is that the Sympoxy bricks are generally much stronger than the other polymer-bricks. However, when the Sympoxy bricks are created by the microwave glovebox method, the specimens turn out to be much weaker.

Both the heated press and vacuum oven methods involve applying pressure during heating, while the microwave does not. This could play a role in the curing process of the Sympoxy. Another possibility is that the polymer does not fully cure in the microwave. Curing involves the formation of covalent bonds, which cause the polymer to harden. This particular polymer cures at 150 ^{o}C and with the microwave method, temperatures cannot be modulated. Furthermore, there was a delicate balance between heating the specimen hot enough and not ruining the mold. Caution had to be taken to not overheat the substrate. Since the bricks held together and appeared to be cured, we moved forward with production under those circumstances. It is possible that only partial curing occurred with microwaved SYM bricks. Eugene Aquino, a colleague working on the same project at International Scientific Technologies, Inc., found the same results concerning the Sympoxy bricks. They were unable to cure Sympoxy using the microwave method.

On another note, the bricks containing PEO break much more quickly and under a lighter load compared to the other bricks. This was expected

because during production quite a few samples broke or did not hold together well. Overall, the brick specimens composed of PCL and PE performed the best during the flexural tests. This is partly due to their thermoplastic nature. Thermoplastic polymers melt rather than cure and their formation process is reversible; they can be re-melted. Conversely, thermoset polymers like Sympoxy, permanently harden when cured due to the formation of chemical bonds. This process is not reversible. Thermoplastic polymers are often more flexible than thermoset polymers because they are held together by secondary intermolecular forces as opposed to covalent bonds which add rigidity.[36] These properties are reflected in the load-deflection curves shown in *Figure 16* and *Figure 17*.

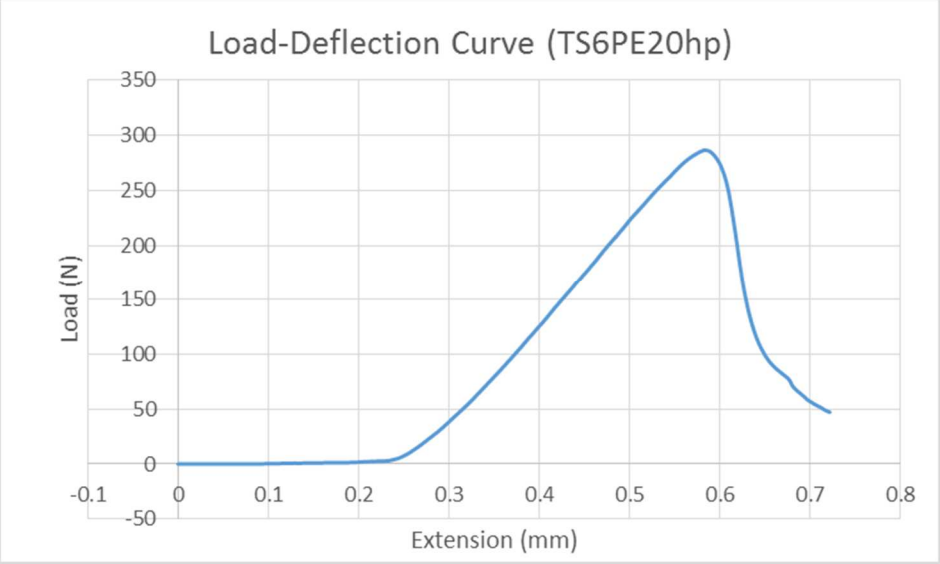

Figure 16. Load-deflection curve for a 20% PE, 80% regolith brick created in the heated press.

Figure 16 depicts the yielding event of a 20% PE brick. At 286.7 N, the brick yields to the applied force, indicated by the maximum point on the curve. The energy stored in the brick dissipates relatively slowly, represented by the decrease in force (negative slope). This curve resembles a classic example of thermoplastic flexural behavior and what occurred for the PCL, PEO, and PE bricks. *Figure 17* depicts the rupturing event of a 20% SYM brick. At 350.73 N, the brick reaches the maximum load it can withstand before snapping in half. This is a quick release of the energy stored by the material and is typical behavior of a thermoset polymer.

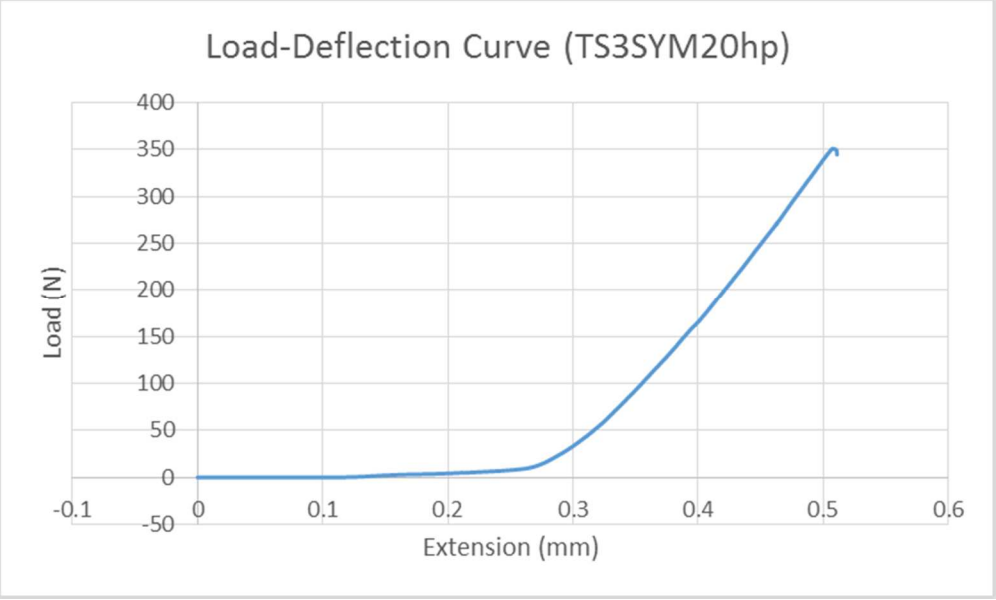

Figure 17. Load-deflection curve for a 20% SYM, 80% regolith brick created in the heated press.

The load values from the flexural tests were used by the instrument's computer to calculate the flexural stress (σ_f) of the materials using the following equation:

$$\sigma_f = \frac{3PL}{2bd^2} \qquad \text{Equation 1.}$$

In this equation, "P" is the load (N) at any point on the load-deflection curve, "L" is the support span (mm), "b" is the width (mm) of the brick tested, and "d" is the depth (mm) of the brick tested.[36] The flexural stress (MPa) represents the maximum stress in the material before yielding/breaking. *Table 4* contains the average flexural stress values that the bricks experience before rupture or yielding. *Table S5* contains all of the maximum flexural stress data points for the samples tested.

Table 4. Average maximum flexural stress values (MPa).

10% Polymer weight, average maximum flexural stress (MPa)				**20% Polymer weight, average maximum flexural stress (MPa)**			
	VO	**HP**	**GB**		**VO**	**HP**	**GB**
PCL	1.316	5.857	1.542	**PCL**	4.205	13.054	6.407
PE	1.038	3.148	1.479	**PE**	4.860	9.736	6.246
PEO	0.408	1.219	0.363	**PEO**	1.943	5.386	2.585
SYM	2.633	3.961	0.536	**SYM**	4.623	11.115	1.756

Trends similar to those noted in the section above are also present in the maximum flexural stress data. PEO bricks have the lowest maximum flexural stress values. The bricks created in the heated press withstand higher stresses before breaking or yielding, as do the 20% polymer bricks compared

to the 10% polymer bricks. PCL bricks perform the best out of the thermoplastic polymers, with the PE bricks experiencing similar results.

Table 5 contains the average maximum flexural extension values (mm) for each brick specimen, calculated using the load-deflection data obtained during flexural tests. *Table S6* contains all of the maximum flexural extension data points for the samples tested.

Table 5. Average maximum flexural extension values (mm).

10% Polymer weight, average maximum flexural extension (mm)				**20% Polymer weight, average maximum flexural extension (mm)**			
	VO	**HP**	**GB**		**VO**	**HP**	**GB**
PCL	1.010	0.632	1.214	**PCL**	2.136	0.721	1.573
PE	0.988	0.719	0.925	**PE**	1.286	0.702	1.164
PEO	0.548	0.580	0.446	**PEO**	0.935	0.754	0.699
SYM	0.803	0.608	0.516	**SYM**	1.055	0.618	0.726

There are some notable trends in this dataset. The bricks that were composed of 20% polymer exhibit larger flexural extensions than the 10% polymer bricks. This is true with the exception of the polyethylene bricks made in the heated press. Theoretically, the addition of a thermoplastic polymer should make the brick exhibit enhanced elastic properties. However, it is important to realize the effect that pressure has on a bricks formation and relating that effect to this data. Both the vacuum oven and microwave brick procedures involve very low applied pressure during the brick formation process relative to the heated press procedure. For PE and PCL, the bricks created in the heated press have extension values smaller than the bricks

created in the vacuum oven and microwave. Since pressure affects the density of a material, a correlation can be drawn between a material's density and its elastic deformation. Furthermore, SYM bricks experience the smallest deformation because it is a harder and more rigid material due to the covalent bonds present in the cured polymer.

Stress-strain curves were also generated from the flexural test data. The elastic modulus was calculated from the slope of the linear portion of these curves. *Figures 18* and *19* show the stress-strain curves for two bricks created in the heated press. The linear highlighted section was used to calculate the slope.

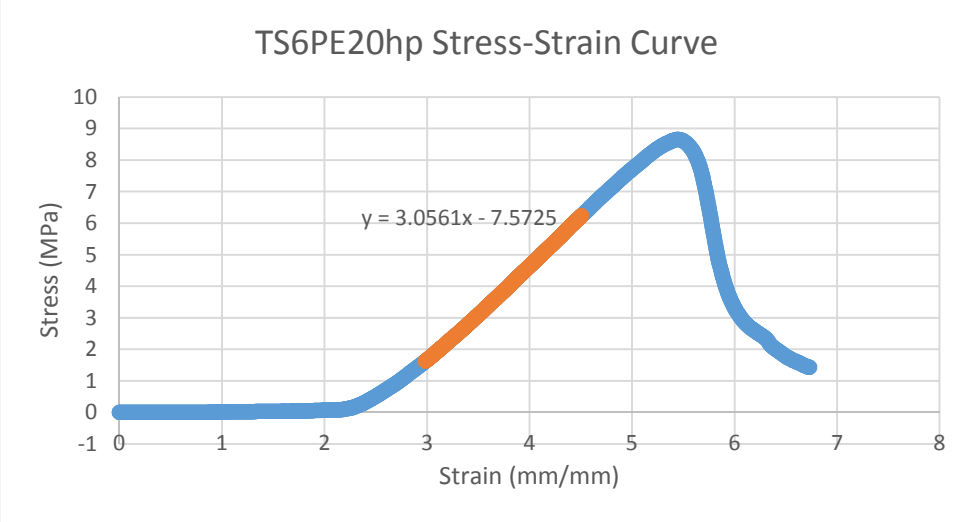

Figure 18. Stress-strain curve of a 20% PE brick created in the heated press. The linear portion (highlighted) is fit with a line of best fit and the equation for that line is displayed.

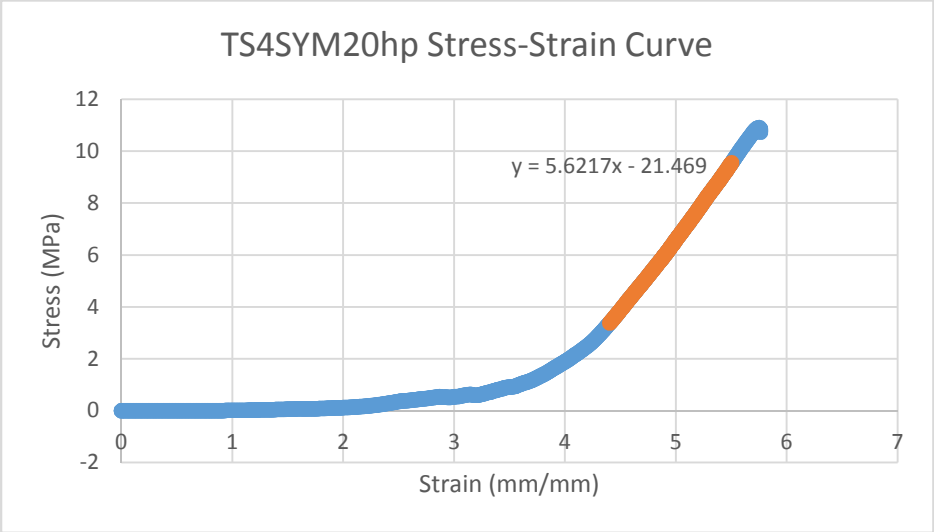

Figure 19. Stress-strain curve of a 20% SYM brick created in the heated press. The linear portion (highlighted) is fit with a line of best fit and the equation for that line is displayed.

Table 6 contains the average elastic modulus values for all of the bricks tested. These values were calculated from the data found in *Table S7.* The bricks created in the heated press exhibit the largest elastic modulus values. Furthermore, the bricks composed of 20% polymer have larger elastic modulus values than those composed of 10% polymer. Materials with low elastic modulus values are known as flexible materials, while materials with high modulus values are known as stiff.[37] Since all of these materials contain polymers, they are relatively flexible compared to what the elastic modulus of a metal would be. Therefore, the bricks made in the heated press are stiffer materials than the bricks made in the vacuum oven and microwave since they exhibit higher elastic modulus values. Increasing the polymer percent also

leads to a larger elastic modulus value. This makes sense since the regolith is loose soil by itself and the polymer acts as a binding agent. More comparisons can be made between the elastic modulus data, but the larger trends that exist are those mentioned above.

Table 6. Table of the average elastic modulus values calculated from the stress-strain curves.

10% Polymer weight, average elastic modulus (MPa)				**20% Polymer weight, average elastic modulus (MPa)**			
	VO	**HP**	**GB**		**VO**	**HP**	**GB**
PCL	0.283	3.318	0.404	**PCL**	0.316	5.270	1.268
PE	0.166	1.672	0.340	**PE**	0.833	3.928	1.319
PEO	0.184	0.691	0.252	**PEO**	0.297	2.516	0.926
SYM	0.505	1.352	0.279	**SYM**	0.600	4.366	0.509

To summarize, the flexural tests conducted using the Instron 5848 Micro Tester were useful for characterizing the flexural and mechanical properties of the bricks created. Additionally, the flexural tests gave valuable insight as to the effectiveness of the three methods used. The bricks composed of PEO performed the worst during the flexural tests, breaking more quickly under lower loads of force. Both PCL and PE brick specimens experienced similar results during flexural tests, producing results at times comparable to the stronger SYM bricks. SYM bricks were the strongest when created in the vacuum oven and heated press. However, the microwave method did not generate strong SYM bricks, most likely due to partial curing. Overall, Sympoxy is not the most attractive polymer for building bricks on Mars

because it's curing process is more temperature and time sensitive than the melting process of the polymers. In this study, the SYM bricks serve well as a control experiment to see how the bricks made from the more ideal polymers compare mechanically to the SYM bricks. Though both PCL and PE bricks showed promising results and comparisons to the SYM bricks, PE remains the more desirable option due to its higher hydrogen content.

The properties of the bricks were enhanced when composed of 20% polymer as opposed to 10%. On Mars, minimizing the need for additional polymer material will be important. In regard to this idea, 10% polymer bricks would be ideal. However, if the shield thickness must be twice as thick to generate the same form of protection a 20% polymer brick would offer, reducing the percent of polymer may not be the best option.

As previously discussed, the heated press produces the best brick substrates due to the applied pressure during heating. Due to weight limitations on a spacecraft, this method is not viable. The vacuum oven and microwave were able to generate good brick substrates that performed well during the flexural tests, making them suitable candidates for methods that could be used in space. They are both lightweight and energy-efficient. An additional mechanism for applying pressure could be added to these methods to improve the properties of the bricks.

OLTARIS

OLTARIS was used to generate radiation analyses to determine the effectiveness of the brick materials against GCR on Mars. It has been shown in many studies, for example Durante in reference 27, that hydrogen is the best element for shielding against GCR. Thus, we predicted the most effective materials would include PE (14.37% H), followed by PEO (9.15% H) and then PCL (8.83% H). However, the calculations involving PEO and PCL did not align with our predictions of what should occur and after rerunning the calculations involving those polymers, nothing changed. For example, the material composed of 10% PEO, 90% REG produces a lower effective dose equivalent value than 20% PEO, 80% REG (see *Figure S1*). Theoretically, more hydrogen content (from the polymer) should improve the effective dose and the material with 20% PEO should be lower. Correspondence with the NASA OLTARIS monitor failed to resolve the issue. Calculating radiation on the Martian surface is a relatively new aspect of the program and could be susceptible to glitches. Since polyethylene is the standard on which other polymers are compared for radiation shielding, we limited our OLTARIS calculations to polyethylene to demonstrate the effectiveness of the polymer and regolith in GCR shielding.

On another hand, the calculations involving PE align theoretically with what was expected and demonstrate the material's ability to shield against GCR. Furthermore, PE is the polymer of choice for radiation shielding due to

its high hydrogen content and will provide the most beneficial analysis for our purposes. The OLTARIS radiation analyses are summarized by the data contained in *Table 7*. Dose (mGy/yr), dose equivalent (leukemia and solid cancer) (mSv/yr), and effective dose equivalent (mSv/yr) were calculated for the materials composed of 100% PE, 20% PE and 80% REG, and 10% PE and 90% REG at different shield thicknesses. The data in *Table 7* is best explained visually and is represented by the following figures: *Figure 20-24*.

Table 7. OLTARIS data for shielding materials containing polyethylene.

PE percent (%)	Dose (mGy/yr)	Dose Equiv. (Leu) (mSv/yr)	Dose Equiv. (Canc) (mSv/yr)	Eff. Dose Equiv. (mSv/yr)	Thickness (cm)	Areal Density (g/cm^2)
100	30.99	58.86	98.60	87.15	10.00	9.20
100	27.15	45.66	71.55	73.22	50.00	46.00
100	23.65	40.26	63.34	64.91	100.00	92.00
20	31.62	69.67	116.30	95.07	10.00	15.44
20	27.06	59.95	99.44	85.43	50.00	77.20
20	21.33	50.48	84.81	72.42	100.00	154.40
10	31.79	73.74	121.00	97.52	10.00	16.22
10	27.21	66.24	108.10	90.08	50.00	81.10
10	21.22	56.01	92.39	76.42	100.00	162.20

Figure 20 depicts the absorbed dose (mGy/yr) as a function of material thickness for the materials composed of 100% PE, 20% PE, and 10% PE. Specifically, the absorbed dose is the dose the astronaut receives after the radiation traverses the shielding material. In general, as shield thickness increases, the absorbed dose decreases. This calculation was run at three different thicknesses: 10 cm, 50 cm, and 100 cm. At 10 cm, the 100% PE

material absorbs a lower dose of GCR, indicating it acts as a better shielding agent. The materials containing 20% PE and 10% PE perform similar to each other. However, for all three materials the difference in absorbed dose is not substantial—less than 1 mGy.

At 50 cm thickness, the materials perform essentially the same, with a max difference of 0.15 mGy. Despite the small difference, the 20% PE material shields the most and leaves the astronaut to absorb 27.06 mGy/yr, while the 10% PE material produces an absorbed dose of 27.21 mGy/yr and the 100% PE material a dose of 27.15 mGy/yr. Notice a shift of shielding performance occurs at 50 cm thickness, where the order of shielding effectiveness decreases in the following order: 20% PE, 100% PE, and then 10% PE. Yet, since the difference in absorbed dose is minimal, no conclusions can be drawn as to what is causing the difference. At a 100 cm thickness, the differences between absorbed dose values increase so that 100% PE produces an absorbed dose ~2 mGy/yr higher than both the 20% and 10% PE materials. Between the latter two materials, the 10% PE material is a more effective shield since the astronaut absorbs a dose of 21.22 mGy/yr, as opposed to a 21.33 mGy/yr dose with the 20% PE material. This data suggests that shielding against GCR is affected by more than just hydrogen content. Furthermore, absorbed dose depends on the shield thickness as well as the material used.

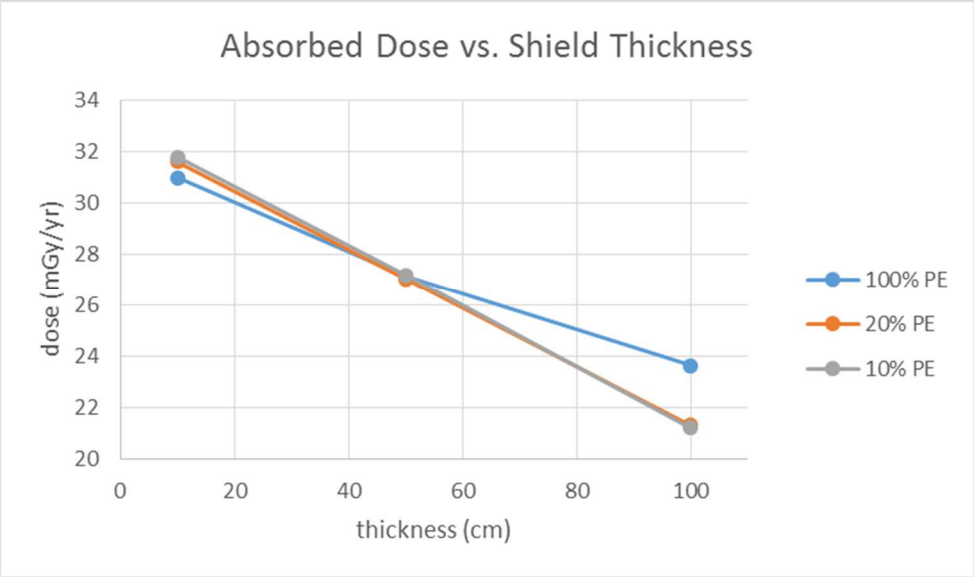

Figure 20. Plot of OLTARIS calculations for the absorbed dose as a function of shield thickness.

Overall, 100% PE shields most effectively at smaller shield thicknesses, but becomes less effective relative to the materials containing Martian regolith at shield thicknesses of 50 cm and 100 cm. Initially, it was thought that the more hydrogen present in the material the better the shield would be, but this data suggests that this is not necessarily true. There are other important components necessary for shielding. For instance, one difference between the materials containing REG and PE, versus only PE, is the density of the material. *Figure 21* plots the absorbed doses for the materials as a function of areal density to further evaluate the differences between the materials and absorbed dose.

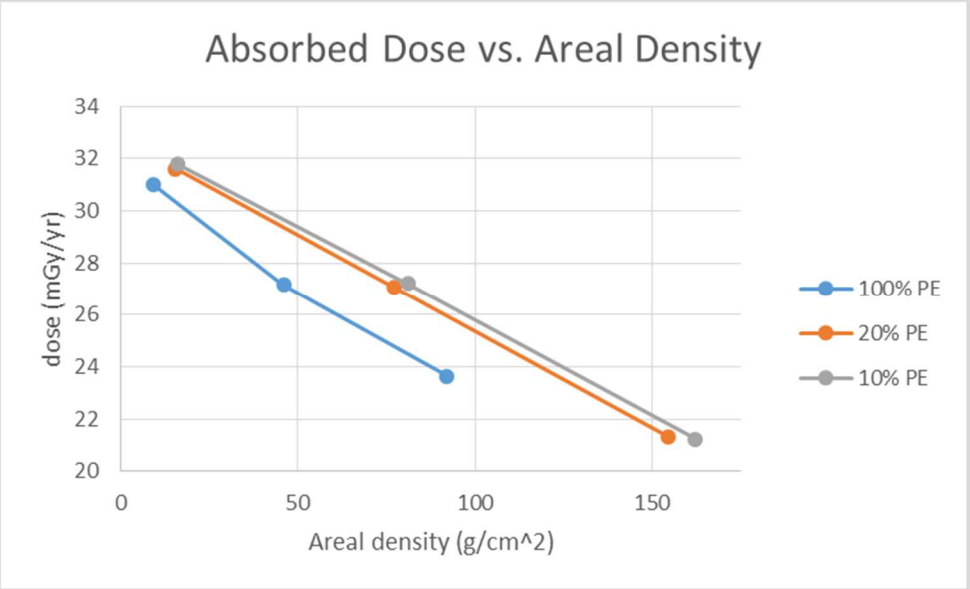

Figure 21. Plot of OLTARIS calculations for absorbed dose as a function of areal density.

Figure 21 makes clearer the distinctions between the three materials and their ability to shield against GCR. The areal densities for the materials shown here are recorded in *Table 7* and correspond to the shield thicknesses of 10 cm, 50 cm, and 100 cm. In this figure the shield thickness increases from the left point to the right point by those defined thickness values. At a 10 cm thickness, the 100% PE material absorbs the lowest dose of GCR and has a slightly smaller areal density than the other materials. As the shield thickness increases to 50 cm, the difference in areal density becomes greater but the absorbed dose is about the same for the materials. When the shield is 100 cm thick, there is significant difference in areal density and a more notable difference in absorbed dose. The materials containing PE and REG have an

areal density of 154.40 g/cm^2 for 20% PE and 162.20 g/cm^2 for 10% PE, whereas the 100% PE material has an areal density of 92.00 g/cm^2. At lower shield thicknesses, it appears that hydrogen content plays a larger role in shielding ability, but as shield thickness increases, the density of the material has a dominant effect.

On a molecular level, there are a couple of explanations for the data presented in *Figures 20* and *21*. First, hydrogen content is important for shielding against GCR, because hydrogen interacts electrostatically with incoming nuclei, absorbing the kinetic energy of the GCR particles without being broken apart. At a shield thickness of 10 cm, this theory is demonstrated. Increased hydrogen content is consistent with lower absorbed doses of GCR, even when the density is lowest for the highest hydrogen containing material. The shield thickness plays an important role because it reduces the absorbed dose. Yet, at larger shield thicknesses, such as at 100 cm, the materials with higher densities exhibit lower absorbed doses than the higher hydrogen content materials. This suggests that the density of the material is important for shielding and while it may not provide Coulombic interactions to slow down the particles, the particles are being slowed by physical interactions with the atoms and molecules. Whether these interactions are causing secondary radiation or not is not within the scope of this study.

Overall, the OLTARIS calculations described above suggest that thicker shields are more effective for protecting astronauts against GCR on the

Martian surface and as shield thickness increases, density becomes more important than hydrogen content. However, the role of hydrogen cannot be dismissed until evaluating the effects of the radiation on the astronaut. Absorbed dose does not account for the damage the radiation causes. Furthermore, it is possible that the material components are important for the type of GCR that passes through the shield.

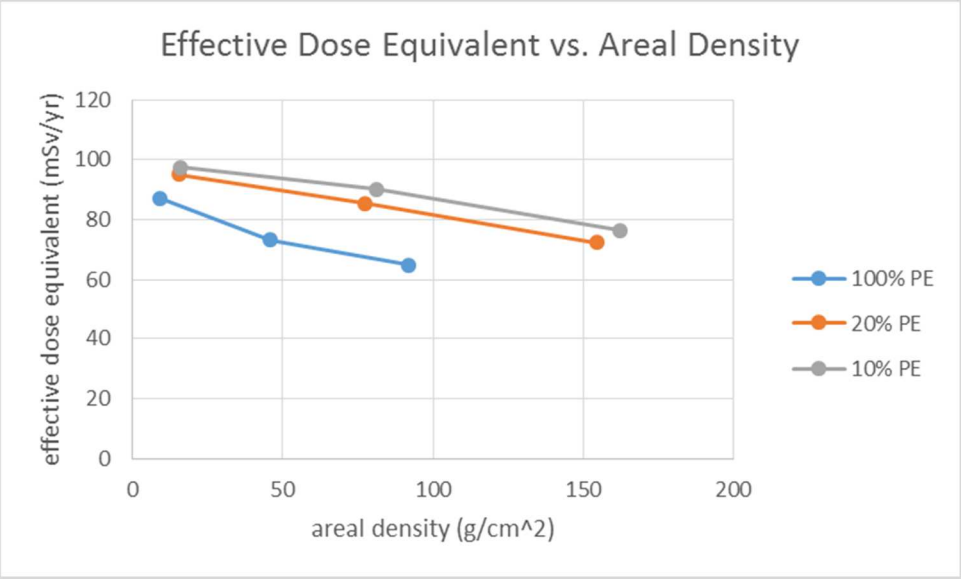

Figure 22. Plot of OLTARIS calculations for effective dose equivalent as a function of areal density.

Figure 22 depicts the relationship between effective dose equivalent (mSv/yr) and areal density (g/cm^2). Effective dose equivalent calculations demonstrate the effectiveness of hydrogen in the shielding material. Overall, at a given shield thickness (10 cm, 50 cm, and 100 cm), the material with the

highest hydrogen content has the lowest effective dose equivalent. The absorbed dose data suggests that the denser the material, the more protection from radiation the astronaut receives. However, this data suggests that protection from more radiation does not correspond to less damage to human tissue. While a thicker shield may block larger quantities of radiation, the intensity of the radiation that does pass through presents the main concern. A lower hydrogen content, denser material may block a higher quantity of lower energy GCR particles, but a smaller number of higher energetic particles may continue to traverse the material. The intensity of these particles imparts more damage to tissue. Ultimately, *Figure 22* demonstrates the importance of hydrogen content in a shielding material. For each of the three shield thicknesses, the effective dose equivalent is lowest for the material containing 100% PE, followed by the 20% PE and then the 10% PE material.

As previously described, effective dose equivalent is a weighted sum of the radiation doses absorbed by human organs. *Table 8* shows an example of the average dose equivalents that the organs of an astronaut would absorb behind a 20% PE, 80% REG material shield that is 32.38 cm thick. These values are weighted based on the organs' susceptibility to radiation. The density of this material is 1.544 g/cm^3 and the thickness of the sphere surrounding the astronaut has an areal density of 50 g/cm^2. Under the previously described parameters, OLTARIS calculates this material to have an effective dose equivalent of 89.15 mSv/yr.

Table 8. Average dose equivalents values for the organs of an astronaut. (20% PE, 80% Martian Regolith, thickness 50 g/cm^2)

Organ	Avg. Dose Equivalent	Per Day	Per Year
Adrenals	2.443E-01 mSv	2.443E-01 mSv/day	8.915E+01 mSv/year
Bladder	2.445E-01 mSv	2.445E-01 mSv/day	8.923E+01 mSv/year
Brain	2.634E-01 mSv	2.634E-01 mSv/day	9.613E+01 mSv/year
Breast	2.653E-01 mSv	2.653E-01 mSv/day	9.684E+01 mSv/year
Colon	2.488E-01 mSv	2.488E-01 mSv/day	9.083E+01 mSv/year
Heart	2.491E-01 mSv	2.491E-01 mSv/day	9.091E+01 mSv/year
Hippocampus	2.602E-01 mSv	2.602E-01 mSv/day	9.496E+01 mSv/year
Kidneys	2.468E-01 mSv	2.468E-01 mSv/day	9.007E+01 mSv/year
Liver	2.495E-01 mSv	2.495E-01 mSv/day	9.107E+01 mSv/year
Lungs	2.611E-01 mSv	2.611E-01 mSv/day	9.530E+01 mSv/year
Ovaries	2.441E-01 mSv	2.441E-01 mSv/day	8.909E+01 mSv/year
Pancreas	2.443E-01 mSv	2.443E-01 mSv/day	8.919E+01 mSv/year
Skin	2.755E-01 mSv	2.755E-01 mSv/day	1.006E+02 mSv/year
Spleen	2.501E-01 mSv	2.501E-01 mSv/day	9.129E+01 mSv/year
Stomach	2.486E-01 mSv	2.486E-01 mSv/day	9.075E+01 mSv/year
Thymus	2.586E-01 mSv	2.586E-01 mSv/day	9.439E+01 mSv/year
Thyroid	2.610E-01 mSv	2.610E-01 mSv/day	9.527E+01 mSv/year
Uterus	2.429E-01 mSv	2.429E-01 mSv/day	8.867E+01 mSv/year
Small Intestine	2.471E-01 mSv	2.471E-01 mSv/day	9.020E+01 mSv/year
Esophagus	2.510E-01 mSv	2.510E-01 mSv/day	9.162E+01 mSv/year
Salivary Glands	2.650E-01 mSv	2.650E-01 mSv/day	9.672E+01 mSv/year
Muscle	2.583E-01 mSv	2.583E-01 mSv/day	9.428E+01 mSv/year
BFO	1.486E-01 mSv	1.486E-01 mSv/day	5.424E+01 mSv/year
Bone	2.566E-01 mSv	2.566E-01 mSv/day	9.366E+01 mSv/year
Lens	2.745E-01 mSv	2.745E-01 mSv/day	1.002E+02 mSv/year
Retina	2.658E-01 mSv	2.658E-01 mSv/day	9.702E+01 mSv/year
Trachea	2.583E-01 mSv	2.583E-01 mSv/day	9.429E+01 mSv/year

Most of the average dose equivalents are relatively close in value. However, each organ does not experience the same effects since some organs are more resistant to radiation than others. *Table 9* contains some of the tissue "weights" that were used for the effective dose equivalent calculation.

Table 9. NASA female nonsmoker tissue weights estimated from the NASA 2010 model for the average U.S. population of nonsmoking females. The weight is directly listed below the organ.[38]

Colon	Stomach	Liver	Lung	Bladder	Breast, Prostate	Ovary, Uterus, Testis	Esophagus
0.093	0.086	0.053	0.322	0.045	0.083	0.067	0.007
Salivary Gland, Oral Cavity	Skin	Thyroid	Bone Marrow	Brain	Bone Surface	Remainder	
0.003	0	0.004	0.138(0.1)	0.016	0	0.083	

Table 9 can be used to understand the contribution of each of the organs' susceptibility to the overall effective dose. The lung has the highest weight at 0.323, whereas the skin has the lowest at 0. These weights were multiplied by the average dose equivalents to generate the total effective dose equivalent.

The last calculation OLTARIS computed was the dose equivalent. To reiterate, this calculation involves weighting the charge of the incoming particle as opposed to the tissue. NASA uses quality factors for the radiation that are multiplied by the absorbed dose to identify the risk of solid cancers and of leukemia. *Figure 23* shows that at each thickness (10 cm, 50 cm, and 100 cm), the risk for developing leukemia is greater than the risk of developing cancer. As the shield's thickness increases, the risk for either cancer or leukemia decreases. Additionally, as hydrogen content increases, the risks for

developing leukemia or cancer also decreases.

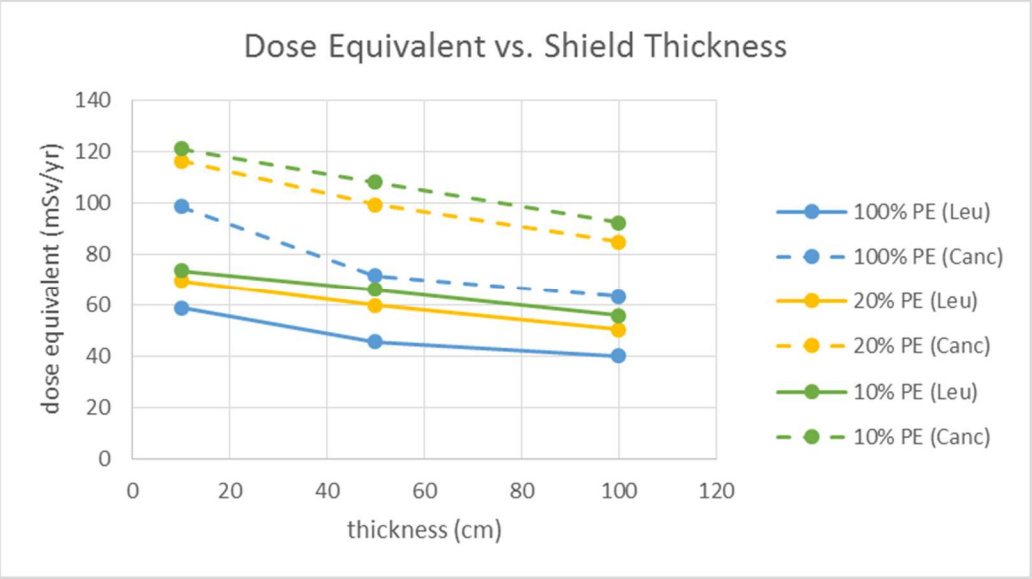

Figure 23. Plot of OLTARIS calculations for dose equivalent as a function of shield thickness.

In summary, OLTARIS calculations were used to predict how the PE brick specimens would perform as radiation shields on Mars. The absorbed dose calculations show that at smaller shield thicknesses, hydrogen content assumes a larger role in blocking radiation. As shield thickness increases, the areal density of the material has a more dominant effect. This information can be used to tune the composition of a shield based on the desired thickness. However, analysis of the effective dose equivalent calculations affirm the necessity for maximizing hydrogen content in a material because it decreases the effective absorbed dose that the astronaut receives. The dose equivalent

calculations depict that the risk for developing cancer on the surface of Mars is higher than the risk of developing leukemia. Yet, the risk for both decreases as shield thickness increases. A comparison between the absorbed dose data, and both the dose equivalent and effective dose equivalent data, show that radiation protection is about quality of protection rather than quantity.

Overall, these calculations indicate that the materials we propose for structural and radiation shielding purposes will offer suitable protection against radiation on Mars. For example, if the total transit to and from Mars generates an exposure of 662 ± 108 mSv, and a 50 cm thick 20% PE, 80% REG shield is used, the effective dose absorbed after 500 days on Mars would be around 123 mSv. In total, the mission to Mars would present an accumulated dose of 785 mSv, which is under 1 Sv. It was mentioned earlier that 1 Sv of accumulated absorbed radiation leads to a 5% increase in fatal cancer.

CONCLUSION

This study presents a novel idea of combining readily available Martian regolith with hydrogen-rich polymers to serve as a structural and radiation shielding material on Mars. Ultimately, materials such as the ones presented in this paper could effectively protect astronauts from GCR, which is the primary deterrent for space habitation. OTLARIS calculations affirm the motivation of using hydrogen-rich polymers for protection against GCR, as they show that effective doses are reduced as hydrogen content is increased. Furthermore,

flexural tests were used to characterize the properties of the bricks. Polyethylene bricks performed well during these tests and so, in addition to it having the highest hydrogen content, the polymer acts as a good binding agent for the brick. Martian regolith alone could not be used a structural material because it will not hold together by itself. With the harsh windstorms and atmospheric conditions on Mars, the polymer is necessary to act as a binding agent for the regolith and to provide protection against GCR.

Lastly, the three methods used in this study were successful in generating bricks. However, due to the weight limitations aboard a spacecraft, the heated press is the least viable option. Both the vacuum oven and microwave are suitable, low-energy mechanisms that form bricks which hold together and perform well during flexural tests.

Appendix

S1. Below is a table containing the dimensions and masses of the bricks created in the vacuum oven.

Date	Brick Name	Width (mm)	Thickness (mm)	Maker	Regolith (g)	Polymer (g)
15-Feb	TS1PCL20	19.029	10.294	Sara	16.025	4.023
15-Feb	TS2PCL20	18.830	10.457	Sara	16.003	4.010
19-Feb	TS3PCL20	19.012	10.790	Sara	16.007	4.031
19-Feb	TS4PCL20	18.800	9.961	Sara	16.049	4.052
20-Feb	TS5PCL20	19.044	10.370	Sara	16.016	4.007
20-Feb	TS6PCL20	18.836	10.874	Sara	16.020	4.025
21-Feb	TS1PCL10	18.829	9.732	Sara	18.008	2.008
21-Feb	TS2PCL10	19.072	9.620	Sara	18.016	2.004
29-Jan	TS3PCL10	19.211	9.790	Liz	18.002	2.003
27-Nov	TS4PCL10	19.434	9.307	Liz	18.001	2.002
27-Nov	TS5PCL10	18.928	10.747	Liz	18.001	2.001
13-Nov	TS6PCL10	19.169	10.164	Liz	18.003	2.002
21-Feb	TS1PEO20	19.010	11.106	Sara	16.013	4.006
21-Feb	TS2PEO20	19.228	10.167	Sara	16.012	4.008
21-Feb	TS3PEO20	18.756	11.270	Sara	16.044	4.007
22-Feb	TS4PEO20	19.023	10.603	Sara	16.038	4.019
22-Feb	TS5PEO20	18.796	10.427	Sara	16.008	4.026
22-Feb	TS6PEO20	19.121	9.646	Sara	16.024	4.013
22-Feb	TS1PEO10	18.838	9.637	Sara	18.014	2.022
22-Feb	TS2PEO10	19.127	9.462	Sara	18.020	2.033
22-Feb	TS3PEO10	19.063	9.414	Sara	18.012	2.013
23-Feb	TS4PEO10	19.024	9.689	Sara	18.014	2.035
23-Feb	TS5PEO10	19.153	9.769	Sara	18.051	2.051
23-Feb	TS6PEO10	18.813	9.684	Sara	18.002	2.003
7-Feb	TS1PE20	19.075	8.818	Sara	16.005	4.009
7-Feb	TS2PE20	18.942	9.846	Sara	16.007	4.003
8-Feb	TS3PE20	18.612	10.496	Sara	16.024	4.051
8-Feb	TS4PE20	18.866	9.038	Sara	16.043	4.028
9-Feb	TS5PE20	19.109	9.155	Sara	16.023	4.007
9-Feb	TS6PE20	18.868	10.781	Sara	16.003	4.005
13-Feb	TS1PE10	18.688	10.352	Sara	18.011	2.011
13-Feb	TS2PE10	18.989	9.939	Sara	18.011	2.007
14-Feb	TS3PE10	18.941	11.298	Julia	18.020	2.013

14-Feb	TS4PE10	18.726	11.392	Julia	18.005	2.008
26-Mar	TS5PE10	19.381	10.030	Liz	18.001	1.999
20-Mar	TS6PE10	18.988	9.040	Liz	18.001	2.001
26-Feb	TS1sym20	19.154	10.640	Sara	16.005	4.003
26-Feb	TS2sym20	19.084	11.110	Sara	15.998	4.002
27-Feb	TS3sym20	19.307	9.793	Sara	16.001	4.010
27-Feb	TS4sym20	18.986	10.163	Sara	16.020	4.004
27-Feb	TS5sym20	19.093	10.353	Sara	16.005	4.009
12-Mar	TS6sym20	19.095	11.220	Sara	16.002	4.000
12-Mar	TS7sym20	18.796	11.465	Sara	15.990	4.002
28-Feb	TS1sym10	19.109	10.506	Sara	18.030	2.046
28-Feb	TS2sym10	19.276	9.859	Sara	18.010	2.002
28-Feb	TS3sym10	18.805	9.823	Sara	18.006	2.001
1-Mar	TS4sym10	19.109	9.511	Sara	18.011	2.014
1-Mar	TS5sym10	18.873	9.301	Sara	18.003	2.001
Mar-18	TS6sym10	19.218	9.227	Sara	18.011	2.019

S2. Below is a table containing the dimensions and masses of the bricks created in the heated hydraulic press.

Date	**Brick Name**	**Width (mm)**	**Thickness (mm)**	**Maker**	**Regolith (g)**	**Polymer (g)**
24-Oct	TS1PCL20	19.056	7.123	Julia	16.010	4.002
31-Oct	TS2PCL20	19.040	7.168	Julia	16.017	4.011
7-Nov	TS3PCL20	19.040	7.296	Julia	16.003	4.003
8-Nov	TS4PCL20	19.040	6.987	Sara	16.007	4.028
9-Nov	TS5PCL20	19.046	6.907	Sara	16.016	4.007
10-Oct	TS6PCL20	19.025	6.969	Julia	15.998	4.001
10-Nov	TS1PCL10	19.070	7.159	Sara	18.008	2.036
14-Nov	TS2PCL10	19.059	8.029	Julia	18.000	2.009
16-Nov	TS3PCL10	19.069	7.432	Sara	18.018	2.020
20-Nov	TS4PCL10	19.079	7.227	Sara	18.011	2.008
27-Nov	TS5PCL10	19.059	7.317	Sara	18.016	2.021
27-Nov	TS6PCL10	19.058	7.714	Julia	18.006	2.008
22-Jan	TS1PEO20	19.279	7.454	Sara	16.007	4.008
22-Jan	TS2PEO20	18.817	7.511	Sara	16.012	4.017
22-Jan	TS3PEO20	19.052	7.287	Sara	16.001	4.000
23-Jan	TS4PEO20	19.049	7.166	Sara	16.015	4.003
23-Jan	TS5PEO20	18.810	7.250	Sara	16.022	4.014
23-Jan	TS6PEO20	19.213	7.309	Sara	16.007	4.004

24-Jan	TS1PEO10	19.069	8.097	Sara	18.018	2.020
24-Jan	TS2PEO10	19.301	8.185	Sara	18.003	2.007
25-Jan	TS3PEO10	19.094	7.425	Sara	18.010	2.008
24-Jan	TS4PEO10	19.056	8.259	Julia	18.010	2.043
24-Jan	TS5PEO10	19.157	8.400	Julia	18.019	2.008
24-Jan	TS6PEO10	18.845	8.385	Julia	18.016	2.001
30-Nov	TS1PE20	19.049	6.798	Sara	16.004	3.999
5-Dec	TS2PE20	18.950	7.446	Julia	16.006	4.001
12-Dec	TS3PE20	19.169	6.994	Sara	16.012	4.000
12-Dec	TS4PE20	19.062	7.000	Sara	16.003	4.003
13-Dec	TS5PE20	19.005	7.767	Sara	16.025	4.006
15-Dec	TS6PE20	19.105	7.573	Julia	16.005	4.004
13-Dec	TS1PE10	19.370	7.950	Sara	18.010	2.049
13-Dec	TS2PE10	18.927	7.986	Sara	18.045	2.011
14-Dec	TS3PE10	19.065	8.346	Sara	18.011	2.027
14-Dec	TS4PE10	19.209	8.450	Sara	18.010	2.012
14-Dec	TS5PE10	18.851	8.430	Sara	18.043	2.009
19-Jan	TS6PE10	19.095	7.435	Sara	18.007	2.005
26-Jan	TS1sym20	19.299	8.066	Sara	16.013	4.003
26-Jan	TS2sym20	18.038	8.057	Sara	16.000	4.023
31-Jan	TS3sym20	18.865	7.908	Sara	16.006	4.004
31-Jan	TS4sym20	19.549	7.606	Sara	16.014	4.005
31-Jan	TS5sym20	19.096	7.593	Sara	16.008	4.009
31-Jan	TS6sym20	19.087	8.449	Julia	16.015	4.017
31-Jan	TS1sym10	19.13	7.425	Julia	18.025	2.011
31-Jan	TS2sym10	18.899	8.654	Julia	18.014	2.000
1-Feb	TS3sym10	19.303	8.696	Sara	18.010	2.005
1-Feb	TS4sym10	18.931	8.357	Sara	18.015	2.009
1-Feb	TS5sym10	19.123	8.242	Sara	18.013	2.000
2-Feb	TS6sym10	19.130	7.425	Sara	18.005	2.004

S3. Below is a table containing the dimensions and masses of the bricks created in the microwave within a CO_2 filled glove box.

Date	**Brick Name**	**Width (mm)**	**Thickness (mm)**	**Maker**	**Regolith (g)**	**Polymer (g)**
2-Oct	TS1PCL20	20.423	8.198	Sara	16.004	4.016
2-Oct	TS2PCL20	20.366	8.200	Sara	16.029	4.014
2-Oct	TS3PCL20	20.363	8.291	Sara	16.065	4.026
2-Oct	TS4PCL20	20.297	8.126	Sara	16.009	3.998

4-Oct	TS5PCL20	20.323	8.359	Sara	16.016	4.037
4-Oct	TS6PCL20	20.352	8.379	Sara	16.016	4.018
5-Oct	TS1PCL10	20.304	8.692	Sara	18.014	2.017
5-Oct	TS2PCL10	20.325	8.742	Sara	18.011	2.005
6-Oct	TS3PCL10	20.336	8.809	Sara	18.011	2.040
6-Oct	TS4PCL10	20.348	8.984	Sara	18.024	2.024
9-Oct	TS5PCL10	20.228	8.426	Sara	18.013	2.026
9-Oct	TS6PCL10	20.360	8.645	Sara	18.003	2.007
22-Sep	TS1PEO20	20.272	8.378	Sara	16.022	4.013
22-Sep	TS2PEO20	20.328	8.448	Sara	16.021	4.046
25-Sep	TS3PEO20	20.358	7.690	Sara	16.031	4.015
25-Sep	TS4PEO20	20.417	8.573	Sara	16.012	4.003
25-Sep	TS5PEO20	20.330	7.941	Sara	16.014	4.031
26-Sep	TS6PEO20	20.304	8.114	Sara	16.012	4.011
27-Sep	TS1PEO10	20.360	8.662	Sara	18.007	2.020
3-Nov	TS2PEO10	20.096	8.909	Sara	18.008	2.027
27-Sep	TS3PEO10	19.285	9.171	Sara	18.018	2.021
28-Sep	TS4PEO10	20.413	8.190	Sara	18.042	2.039
29-Sep	TS5PEO10	20.264	8.394	Sara	18.013	2.033
29-Sep	TS6PEO10	20.421	8.278	Sara	18.001	2.005
18-Sep	TS1PE20	20.000	8.551	Sara	16.024	4.001
18-Sep	TS2PE20	20.140	8.356	Sara	16.006	4.002
18-Sep	TS3PE20	20.019	8.358	Sara	16.000	4.009
18-Sep	TS4PE20	20.153	8.169	Sara	16.029	4.012
19-Sep	TS5PE20	20.036	7.980	Sara	16.022	4.029
19-Sep	TS6PE20	20.179	8.682	Sara	16.073	4.017
19-Sep	TS1PE10	20.277	9.516	Sara	18.030	2.005
20-Sep	TS2PE10	20.308	8.703	Sara	18.045	2.003
20-Sep	TS3PE10	20.315	8.782	Sara	18.005	2.005
21-Sep	TS4PE10	20.281	9.176	Sara	18.013	2.043
21-Sep	TS5PE10	20.193	9.118	Sara	18.016	2.030
22-Sep	TS6PE10	20.252	8.826	Sara	18.005	2.011
10-Oct	TS1sym20	20.399	9.313	Sara	16.025	4.009
11-Oct	TS2sym20	20.353	9.752	Sara	16.021	4.010
11-Oct	TS3sym20	20.572	9.330	Sara	16.007	4.009
12-Oct	TS4sym20	20.423	9.153	Sara	16.012	4.003
13-Oct	TS5sym20	20.009	10.494	Sara	16.008	4.003
18-Oct	TS6sym20	20.147	9.690	Sara	16.039	4.023
19-Oct	TS1sym10	20.189	9.120	Sara	18.022	2.005

19-Oct	TS2sym10	20.175	8.873	Sara	18.019	2.002
26-Oct	TS3sym10	20.057	9.204	Sara	18.032	2.026
26-Oct	TS4sym10	20.112	8.997	Sara	18.003	2.014
27-Oct	TS5sym10	20.291	8.872	Sara	18.005	2.030
30-Oct	TS6sym10	19.902	8.967	Sara	18.030	2.003

S4. This table contains the maximum load values (N) for the bricks constructed in the vacuum oven under low CO_2 atmospheric pressure, in the heated hydraulic press, and in the microwave in the CO_2-filled glove box. The row beginning with TS1 represents the trial sample and the column on the far left contains the name of the brick, which includes the polymer type, percent of polymer used, and the method in which it was made. The following samples were removed after statistical analysis confirmed them as outliers: TS5PCL10hp, TS6PE10hp, TS6Sym10hp, TS1Sym20hp, and TS4PCL10gb. Averages of the load values were calculated without the outliers and are represented in *Table 3*..

Maximum Load (N) for the vacuum oven bricks							
	TS1	**TS2**	**TS3**	**TS4**	**TS5**	**TS6**	**Average**
PCL10vo	75.844	55.284	48.759	71.755	109.686	89.142	75.078
PCL20vo	253.046	331.610	218.870	274.361	269.703	218.061	260.942
PE10vo	59.180	53.670	69.239	69.157	79.266	59.863	65.063
PE20vo	206.710	203.262	209.893	284.030	314.623	323.914	257.072
PEO10vo	25.529	28.565	24.764	10.884	21.890	16.507	21.357
PEO20vo	59.947	163.447	97.601	100.182	114.081	151.860	114.520
Sym10vo	216.499	193.884	99.470	112.185	98.570	148.778	144.898
Sym20vo	254.058	205.801	271.213	322.783	379.643	328.634	293.689
Maximum Load (N) for the heated press bricks							
	TS1	**TS2**	**TS3**	**TS4**	**TS5**	**TS6**	**Average**
PCL10hp	175.303	179.668	168.838	224.624	123.865	196.571	189.001
PCL20hp	360.834	412.299	425.743	353.990	356.751	349.055	376.445
PE10hp	124.390	121.621	138.564	103.983	124.474	179.557	122.606
PE20hp	285.782	276.957	260.533	317.701	340.114	286.693	294.630
PEO10hp	30.449	48.617	57.177	35.686	42.856	46.703	43.581
PEO20hp	216.893	201.372	178.239	172.663	107.058	126.304	167.088
Sym10hp	180.250	175.931	155.624	156.427	160.964	239.782	165.839
Sym20hp	85.072	230.348	350.730	373.031	469.094	526.957	390.032
Maximum Load (N) for the glove box bricks							
	TS1	**TS2**	**TS3**	**TS4**	**TS5**	**TS6**	**Average**
PCL10gb	69.353	73.617	66.196	96.047	74.736	70.386	70.858
PCL20gb	227.572	260.078	249.556	281.494	316.794	277.302	268.799

PE10gb	80.097	74.686	70.115	81.289	63.648	72.009	73.641
PE20gb	247.251	254.590	234.867	287.253	279.409	265.586	261.493
PEO10gb	20.733	14.852	15.062	22.828	11.375	12.694	16.257
PEO20gb	106.256	103.704	99.335	88.551	121.091	115.443	105.730
Sym10gb	23.996	22.232	34.822	23.427	31.741	22.540	26.460
Sym20gb	93.198	83.103	89.403	124.397	58.920	137.048	97.678

S5. This table contains the maximum flexural stress values (MPa or N/mm^2) for the bricks constructed in: the vacuum oven under low CO_2 atmospheric pressure, the heated hydraulic press, and the microwave in the CO_2-filled glove box. The row beginning with TS1 represents the trial sample and the column on the far left contains the name of the brick, which includes the polymer type, percent of polymer used, and the method in which it was made. The following samples were removed after statistical analysis confirmed them as outliers: TS5PCL10hp, TS6PE10hp, TS6Sym10hp, TS1Sym20hp, and TS4PCL10gb. Averages of the maximum flexural stress were calculated without the outliers and are represented in *Table 4.*

Maximum flexural stress (MPa) for the vacuum oven bricks							
	TS1	**TS2**	**TS3**	**TS4**	**TS5**	**TS6**	**Average**
PCL10vo	1.408	1.037	0.890	1.411	1.661	1.490	**1.316**
PCL20vo	4.154	5.332	3.273	4.869	4.360	3.241	**4.205**
PE10vo	0.978	0.735	0.948	0.942	1.346	1.277	**1.038**
PE20vo	4.614	3.664	3.389	6.101	6.503	4.890	**4.860**
PEO10vo	0.483	0.573	0.485	0.202	0.396	0.310	**0.408**
PEO20vo	0.846	2.722	1.356	1.551	2.358	2.826	**1.943**
Sym10vo	3.398	3.426	1.815	2.149	1.999	3.010	**2.633**
Sym20vo	3.879	2.892	4.849	5.449	6.141	4.526	**4.623**
Maximum flexural stress (MPa) for the heated press bricks							
	TS1	**TS2**	**TS3**	**TS4**	**TS5**	**TS6**	**Average**
PCL10hp	5.938	4.841	5.307	7.462	4.019	5.738	**5.857**
PCL20hp	12.355	13.952	13.906	12.608	12.998	12.506	**13.054**
PE10hp	3.364	3.336	3.454	2.510	3.076	5.631	**3.148**
PE20hp	10.747	8.727	9.198	11.260	9.821	8.662	**9.736**
PEO10hp	0.806	1.245	1.798	0.909	1.390	1.167	**1.219**
PEO20hp	6.703	6.280	5.833	5.843	3.585	4.074	**5.386**
Sym10hp	4.144	4.115	3.529	3.917	4.102	7.527	**3.961**
Sym20hp	2.243	7.926	9.822	10.919	14.105	12.803	**11.115**
Maximum flexural stress (MPa) for the glove box bricks							
	TS1	**TS2**	**TS3**	**TS4**	**TS5**	**TS6**	**Average**
PCL10gb	1.497	1.569	1.389	1.936	1.723	1.531	**1.542**

PCL20gb	5.489	6.287	5.902	6.953	7.386	6.425	**6.407**
PE10gb	1.444	1.607	1.481	1.576	1.255	1.511	**1.479**
PE20gb	5.597	5.993	5.781	7.071	7.250	5.780	**6.246**
PEO10gb	0.449	0.308	0.307	0.552	0.264	0.300	**0.363**
PEO20gb	2.472	2.366	2.732	1.954	3.127	2.859	**2.585**
Sym10gb	0.473	0.463	0.678	0.476	0.658	0.466	**0.536**
Sym20gb	1.744	1.421	1.653	2.407	0.913	2.398	**1.756**

S6. This table contains the maximum flexural extension values (mm) for the bricks constructed in: the vacuum oven under low CO_2 atmospheric pressure, the heated hydraulic press, and the microwave in the CO_2-filled glove box. The row beginning with TS1 represents the trial sample and the column on the far left contains the name of the brick, which includes the polymer type, percent of polymer used, and the method in which it was made. The following samples were removed after statistical analysis confirmed them as outliers: TS5PCL10hp, TS6PE10hp, TS6Sym10hp, TS1Sym20hp, and TS4PCL10gb. Averages of the maximum flexural extension were calculated without the outliers and are represented in *Table 5*.

Maximum flexural extension (mm) for the vacuum oven bricks							
	TS1	**TS2**	**TS3**	**TS4**	**TS5**	**TS6**	**Average**
PCL10vo	0.866	0.603	1.329	0.836	1.219	1.206	**1.010**
PCL20vo	1.859	2.626	1.821	3.126	2.145	1.240	**2.136**
PE10vo	0.799	0.915	1.091	1.443	0.872	0.810	**0.988**
PE20vo	0.677	0.739	1.330	0.951	1.126	2.891	**1.286**
PEO10vo	0.556	0.839	0.532	0.321	0.681	0.357	**0.548**
PEO20vo	0.918	1.007	1.162	0.913	0.761	0.850	**0.935**
Sym10vo	0.946	0.795	0.687	0.742	0.892	0.754	**0.803**
Sym20vo	1.011	0.952	0.906	1.028	1.147	1.287	**1.055**
Maximum flexural extension (mm) for the heated press bricks							
	TS1	**TS2**	**TS3**	**TS4**	**TS5**	**TS6**	**Average**
PCL10hp	0.723	0.438	0.645	0.612	0.893	0.741	**0.632**
PCL20hp	0.561	0.641	0.796	0.809	0.536	0.981	**0.721**
PE10hp	0.821	0.729	0.591	0.927	0.527	0.754	**0.719**
PE20hp	0.787	0.769	0.507	0.855	0.574	0.721	**0.702**
PEO10hp	0.460	0.718	0.458	0.641	0.737	0.465	**0.580**
PEO20hp	0.676	0.703	0.790	0.813	0.663	0.877	**0.754**
Sym10hp	0.549	0.547	0.771	0.497	0.677	0.506	**0.608**
Sym20hp	0.680	0.385	0.511	0.615	0.806	0.771	**0.618**
Maximum flexural extension (mm) for the glove box bricks							
	TS1	**TS2**	**TS3**	**TS4**	**TS5**	**TS6**	**Average**

PCL10gb	0.898	1.030	1.409	0.987	1.589	1.143	**1.214**
PCL20gb	1.099	1.437	1.325	2.153	1.582	1.844	**1.573**
PE10gb	0.851	0.872	1.130	0.876	0.770	1.052	**0.925**
PE20gb	1.000	1.079	1.254	1.519	1.111	1.021	**1.164**
PEO10gb	0.591	0.410	0.390	0.476	0.431	0.377	**0.446**
PEO20gb	0.809	0.640	0.619	0.780	0.828	0.519	**0.699**
Sym10gb	0.589	0.473	0.396	0.679	0.464	0.491	**0.516**
Sym20gb	0.576	0.705	1.037	0.589	0.952	0.499	**0.726**

S7. This table contains the average elastic modulus values (recorded in *Table 6)* for the bricks constructed in: the vacuum oven under low CO_2 atmospheric pressure, the heated hydraulic press, and the microwave in the CO_2-filled glove box. The row beginning with TS1 represents the trial sample and the column on the far left contains the name of the brick, which includes the polymer type, percent of polymer used, and the method in which it was made.

Average modulus of elasticity (MPa) for the vacuum oven bricks.							
	TS1	**TS2**	**TS3**	**TS4**	**TS5**	**TS6**	**Average**
PCL10vo	**0.328**	**0.418**	**0.209**	**0.365**	**0.229**	**0.152**	**0.283**
PCL20vo	**0.358**	**0.360**	**0.354**	**0.267**	**0.301**	**0.257**	**0.316**
PE10vo	**0.144**	**0.206**	**0.132**	**0.087**	**0.174**	**0.253**	**0.166**
PE20vo	**1.855**	**0.785**	**0.292**	**1.065**	**0.827**	**0.174**	**0.833**
PEO10vo	**0.179**	**0.214**	**0.275**	**0.120**	**0.167**	**0.147**	**0.184**
PEO20vo	**0.175**	**0.397**	**0.149**	**0.200**	**0.400**	**0.464**	**0.297**
Sym10vo	**0.411**	**0.483**	**0.413**	**0.510**	**0.587**	**0.626**	**0.505**
Sym20vo	**0.483**	**0.378**	**1.034**	**0.710**	**0.640**	**0.354**	**0.600**
Average modulus of elasticity (MPa) for the heated press bricks.							
	TS1	**TS2**	**TS3**	**TS4**	**TS5**	**TS6**	**Average**
PCL10hp	**3.908**	**2.507**	**3.476**	**3.887**	**3.024**	**3.107**	**3.318**
PCL20hp	**4.869**	**5.435**	**4.759**	**5.559**	**6.126**	**4.873**	**5.270**
PE10hp	**1.606**	**1.895**	**1.282**	**0.924**	**1.332**	**2.994**	**1.672**
PE20hp	**4.783**	**3.272**	**4.356**	**5.038**	**3.123**	**2.993**	**3.928**
PEO10hp	**0.573**	**0.570**	**1.142**	**0.362**	**0.797**	**0.702**	**0.691**
PEO20hp	**2.672**	**1.845**	**2.989**	**3.174**	**2.250**	**2.164**	**2.516**
Sym10hp	**1.586**	**1.292**	**0.798**	**1.547**	**1.536**	**4.074**	**1.352**
Sym20hp	**2.493**	**4.082**	**4.557**	**5.626**	**5.853**	**3.587**	**4.366**
Average modulus of elasticity (MPa) for the glove box bricks.							
	TS1	**TS2**	**TS3**	**TS4**	**TS5**	**TS6**	**Average**

PCL10gb	**0.370**	**0.524**	**0.248**	**0.573**	**0.403**	**0.307**	**0.404**
PCL20gb	**1.353**	**1.218**	**1.045**	**1.501**	**1.561**	**0.932**	**1.268**
PE10gb	**0.347**	**0.368**	**0.341**	**0.299**	**0.295**	**0.393**	**0.340**
PE20gb	**1.144**	**1.255**	**1.646**	**1.192**	**1.521**	**1.154**	**1.319**
PEO10gb	**0.234**	**0.245**	**0.228**	**0.303**	**0.215**	**0.289**	**0.252**
PEO20gb	**0.971**	**0.633**	**1.183**	**0.541**	**1.067**	**1.163**	**0.926**
Sym10gb	**0.203**	**0.209**	**0.437**	**0.271**	**0.317**	**0.237**	**0.279**
Sym20gb	**0.645**	**0.269**	**0.562**	**0.734**	**0.301**	**0.545**	**0.509**

Figure S1. Plot of effective dose equivalent values as a function of areal density. The points move from left to right with decreasing polymer percentages (100%, 20%, and 10%). Each calculation occurred at a shield thickness of 50 cm.

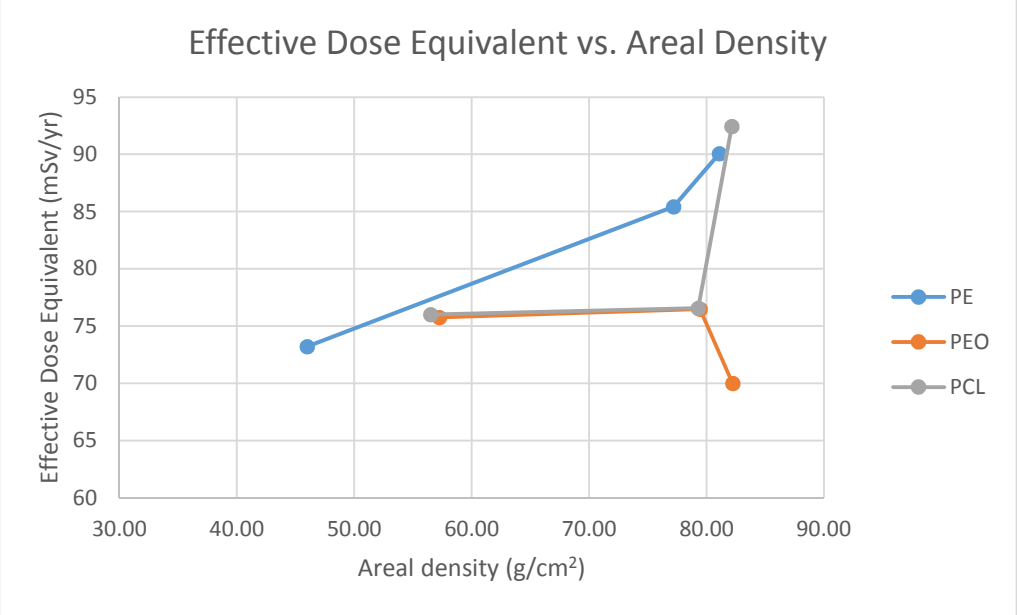

REFERENCES

[1] Apollo 11 Moon Landing. https://www.jfklibrary.org/JFK/JFK-Legacy/Apollo_11_Moon_Landing.aspx, (June 30, 2017), *John F. Kennedy Presidential Library and Museum*.
[2] Erickson, K.; Leon, N. NASA Space Place Explore Earth and Space. https://spaceplace.nasa.gov/moon-distance/en/ (Novermber 20, 2017)
[3] Redd, N. T. How Long Does It Take to Get to Mars?. www.space.com/24701-how-long-does-it-take-to-get-to-mars.html (November 4, 2017).
[4] NASA. How long would a trip to Mars take?. image.gsfc.nasa.gov/poetry/venus/q2811.html (November 20, 2017).
[5] Choi, C. Q. How NASA Would Send Humans on Mars. https://www.space.com/7029-nasa-send-humans-mars.html (June 30, 2017).
[6] Gushanas, T. Why Space Radiation Matters. https://www.nasa.gov/analogsnsrl/why-space-radiation-matters (July 25, 2017).
[7] Lankford, M. What is space radiation?. https://srag.jsc.nasa.gov/SpaceRadiation/What/What.cfm (November 15, 2017).
[8] Nagaraja, M. P. Heliosphere. https://science.nasa.gov/heliophysics/focus-areas/heliosphere (April 28, 2018).
[9] Stern, D. P.; Peredo, M. Solar Energetic Particles." https://www-spof.gsfc.nasa.gov/Education/wsolpart.html (April 28, 2018).
[10] Lankford, M. What is space radiation?. https://srag.jsc.nasa.gov/SpaceRadiation/What/What.cfm (November 15, 2017).
[11] Fox, K. C. Solar Minimum; Solar Maximum. www.nasa.gov/mission_pages/sunearth/news/solarmin-max.html (November 17, 2017).
[12] Chappel, L. J.; Cucinotta, F. A.; Kim, M. Y. Space Radiation Cancer Risk Projections and Uncertainties—2012. https://spaceradiation.jsc.nasa.gov/irModels/TP-2013-217375.pdf (April 28, 2018).
[13] Christian, E. R. Galactic Cosmic Rays. https://helios.gsfc.nasa.gov/gcr.html (June 30, 2017).
[14] Lin, R. P. Energetic Particles in Space. *Sol Phys* **1980,** 67: 393. https://doi.org/10.1007/BF00149816
[15] Meyers, J. D. Cosmic Rays. imagine.gsfc.nasa.gov/science/objects/cosmic_rays2.html (October 15, 2017).
[16] Doses in Our Daily Lives. www.nrc.gov/about-nrc/radiation/around-us/doses-daily-lives.html (April 20, 2018), United States Nuclear Regulatory Commission.

[17] NASA facts: Understanding Space Radiation. https://spaceflight.nasa.gov/spacenews/factsheets/pdfs/radiation.pdf (October 20, 2017).
[18] Frazier, S.; Garner, R. How to Protect Astronauts from Space Radiation on Mars. www.nasa.gov/feature/goddard/real-martians-how-to-protect-astronauts-from-space-radiation-on-mars (October 20, 2017).
[19] Types of Radiation in Space. https://www.nasa.gov/sites/default/files/np-2014-03-001-jsc-orion_radiation_handout.pdf (April 20, 2018).
[20] Gifford, S. E. Calculated Risks: How Radiation Rules Manned Mars Exploration. www.space.com/24731-mars-radiation-curiosity-rover.html (October 20, 2017).
[21] Zeitlin, C., Hassler, D. M. et al. Measurements of Energetic Particle Radiation in Transit to Mars on the Mars Science Laboratory. *Science* **2013,** Vol. 340, Issue 6136, pp. 1080-1084. DOI: 10.1126/science.1235989
[22] Perrotto, T. J.; Schmid, D.; Dunbar, B. Radiation Measured by NASA's Curiosity on Voyage to Mars has Implications for Future Human Missions. www.nasa.gov/home/hqnews/2013/may/HQ_13-165_MSL_Radiation_Findings.html (October 15, 2017).
[23] Gifford, S. E. Calculated Risks: How Radiation Rules Manned Mars Exploration. www.space.com/24731-mars-radiation-curiosity-rover.html (October 20, 2017).
[24] Copeland, S. The Deep Space Radiation Environment. large.stanford.edu/courses/2012/ph241/copeland2/ (October 15, 2017).
[25] Materials Used in Radiation Shielding. www.thomasnet.com/articles/custom-manufacturing-fabricating/radiation-shielding-materials/ (October 20, 2017). *ThomasNet® - Product Sourcing and Supplier Discovery Platform*.
[26] Durante, M. Space radiation protection: Destination Mars. *Life Sciences in Space Research*, **2014**, *vol. 1*, doi:10.1016/j.lssr.2014.01.002.
[27] Williams, D. R. Mars Fact Sheet. nssdc.gsfc.nasa.gov/planetary/factsheet/marsfact.html (November 10, 2017).
[28] Williams, D. R. Earth Fact Sheet. nssdc.gsfc.nasa.gov/planetary/factsheet/earthfact.html (November 10, 2017).
[29] Allen, C. C.; et al. JSC Mars-1 - Martian regolith simulant. *Lunar and Planetary Science XXIX*. https://www.lpi.usra.edu/meetings/LPSC98/pdf/1690.pdf (October 15, 2017).
[30] Beegle, L.W., Peters, G.H., Mungas, G.S., Bearman, G.H., Smith, J.A. and Anderson, R.C. Mojave Martian Simulant: A New Martian Soil Simulant. *Lunar and Planetary Science XXXVIII* [online] **2007,** https://www.lpi.usra.edu/meetings/lpsc2007/pdf/2005.pdf.
[31] Steigerwald, B. NASA Goddard Instrument's First Detection of Organic Matter on Mars. www.nasa.gov/content/goddard/mars-organic-matter (October 15, 2017).

[32] ULTEM™ Resin.www.sabic.com/en/products/specialties/ultem-resins/ultem-resin (April 20, 2017).
[33] Load Cell. www.instron.us/en-us/our-company/library/glossary/l/load-cell (April 4, 2018).
[34] Test Methods for Flexural Properties of Unreinforced and Reinforced Plastics and Electrical Insulating Materials. ASTM International **2003**, doi:10.1520/d0790-15e02.
[35]Chappel, L. J.; Cucinotta, F. A.; Kim, M. Y. Space Radiation Cancer Risk Projections and Uncertainties—2012. https://spaceradiation.jsc.nasa.gov/irModels/TP-2013-217375.pdf (April 28, 2018).
[36] Callister, W. D. *Materials Science and Engineering An Introduction*, Seventh Edition; John Wiley and Sons, Inc.: New York, 2007; ISBN-13:978-0-471-73696-7.
[37] High Vs. Low Modulus Of Elasticity. www.covascientific.com/blog/high-vs.-low-modulus-of-elasticity (April 28, 2018).
[38] Chappel, L. J.; Cucinotta, F. A.; Kim, M. Y. Space Radiation Cancer Risk Projections and Uncertainties—2012. https://spaceradiation.jsc.nasa.gov/irModels/TP-2013-217375.pdf (April 28, 2018).